Charge symmetric systems ^{12}C+^{13}N and ^{12}C+^{13}C with the orthogonalized coupled-reaction-channel method

B. Imanishi and V. Denisov*

Institute for Nuclear Study, University of Tokyo, Tanashi, Tokyo 188, Japan

T. Motobayashi

Department of Physics, Rikkyo University, Toshima-ku, Tokyo 171, Japan

(Received 17 October 1996)

The charge symmetric scattering systems ^{12}C+^{13}N and ^{12}C+^{13}C have been investigated by using the orthogonalized coupled-reaction-channel (OCRC) method with the basis functions of the elastic, inelastic, and transfer channels defined by the single-particle states, $1p\frac{1}{2}$, $2s\frac{1}{2}$, $1d\frac{5}{2}$, and $1d\frac{3}{2}$ of the valence nucleon in ^{13}N or ^{13}C. The data of the elastic scattering of ^{13}N on ^{12}C measured by Liénard *et al.* have been explained consistently with the data of the elastic and inelastic scattering of the ^{12}C+^{13}C system. The CRC effects on both of the above systems are very strong, although those on the ^{12}C+^{13}N system are fairly weaker than the ^{12}C+^{13}C system. The role of the highly excited single-particle states $1d\frac{3}{2}$ is particularly important in the formation of a specific CRC scheme, i.e., the formation of the covalent molecules due to the hybridization caused by the mixing of the different parity single-particle states. The fusion cross sections of the ^{12}C+^{13}C system at energies below the Coulomb barrier are strongly enhanced as a result of the strong CRC effects as compared with those of the ^{12}C+^{12}C system, while in ^{12}C+^{13}N system the enhancement of the sub-barrier fusion has not been observed. The above absorption mechanism for the ^{12}C+^{13}C system explains the lack of the molecular-resonance phenomena observed in the ^{12}C+^{12}C system. We check the effects of the dipole ($E1$) transition of the valence nucleon in ^{13}N (and also in ^{13}C) due to the core-core Coulomb interaction in the scattering at sub-barrier energies. The effects are not appreciable. [S0556-2813(97)03104-X]

PACS number(s): 24.10.Eq, 25.70.−z, 24.30.−v, 27.20.+n

I. INTRODUCTION

Heavy-ion reactions induced by unstable nuclei present us with new possibilities not only in the developments of our knowledge on nuclear reactions investigated so far but also with new studies of the reaction mechanisms not accessible with stable nuclei [1]. Verification of the charge symmetry in heavy ion reactions is one of such problems, as the use of unstable nuclei makes it possible to realize mirror scattering systems.

Recently Liénard *et al.* [2] have measured angular distributions of the elastic scattering of the unstable nucleus ^{13}N on ^{12}C at energies 7.824, 9.6, and 14.16 MeV in the center of mass. The ^{13}N nucleus contains a valence nucleon, which is weakly bound around the core nucleus ^{12}C, and the excited states of the valence nucleon lie in the continuum energy region as resonance states. This may strongly induce inelastic transitions and transfers of the valence nucleon, resulting in the formation of nucleonic molecular orbitals around the two core (^{12}C) nuclei at energies around the Coulomb barrier [3–7].

The data have been analyzed by employing the optical-potential model with the inclusion of the elastic transfers of the valence nucleon and have been compared with the analysis for the ^{12}C+^{13}C system, which is the charge symmetric

partner of the above [2]. The result shows that the depth of the imaginary potential for the ^{12}C+^{13}N system is much shallower than that for the ^{12}C+^{13}C system by a factor of about $\frac{1}{3}$–$\frac{1}{5}$. Namely the optical potentials obtained are not charge symmetric. The authors in Ref. [2] argue that the loss of the charge symmetry is partly due to a smaller number of two-fragment channels available for the absorption into direct channels for the ^{12}C+^{13}N system.

Another possible cause for the charge asymmetry is the different decay schemes of the compound nuclei ^{25}Mg and ^{25}Al. In Fig. 1 we see the decay mode of the compound nucleus ^{25}Al formed by the ^{12}C+^{13}N reaction and that of the compound nucleus ^{25}Mg by the ^{12}C+^{13}C reaction. The decay probability of the compound nucleus ^{25}Al seems to be slightly larger than that of the compound nucleus ^{25}Mg at the energies near or below the Coulomb barriers of the above systems. However, it is questionable that such small difference of the decay modes can give rise to such a big difference of the imaginary parts of the optical potentials as pointed out by Liénard *et al.* [2].

In this paper we concentrate our attention on the direct-reaction mechanisms of the ^{12}C+^{13}C and ^{12}C+^{13}N systems. To do this, we perform calculations with the orthogonalized coupled-reaction-channel (OCRC) theory which has been formulated in Ref. [5] so as to relate the CRC method to the molecular-orbital model of valence nucleons. If we include, in the OCRC analysis, sufficient number of the channels concerned with the single-particle states of the valence nucleon, a part of the charge symmetry of the optical potential should be restored in the calculation.

————
*Permanent address: Institute for Nuclear Research, Prospect Nauki 47, 252028 Kiev, Ukraine.
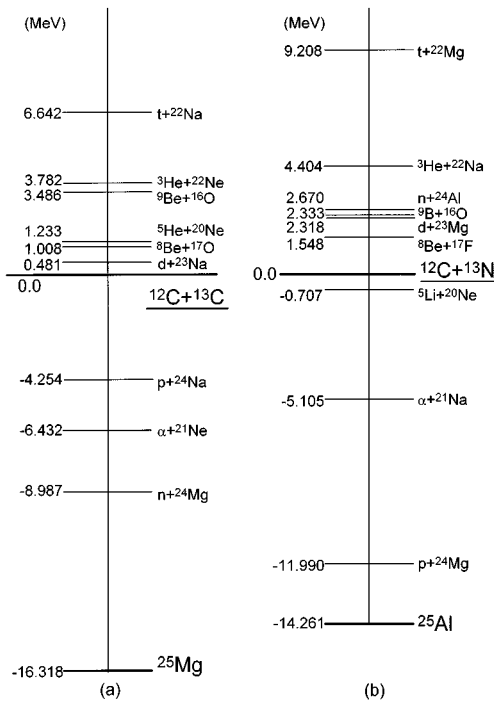
FIG. 1. Two fragment decay schemes of (a) the compound nucleus ^{25}Al of the ^{12}C+^{13}C system and (b) the compound nucleus ^{25}Mg of the ^{12}C+^{13}N system.

We employ the channels related to the states ^{13}N[gr. $\frac{1}{2}^-$; 2.36 MeV, $\frac{1}{2}^+$ (resonance state); 3.55 MeV, $\frac{5}{2}^+$ (resonance state); 7.9 MeV, $\frac{3}{2}^+$ (resonance state)] for the ^{12}C+^{13}N system and those related to the ^{13}C[gr. $\frac{1}{2}^-$; 3.09 MeV, $\frac{1}{2}^+$; 3.85 MeV, $\frac{5}{2}^+$; 8.2 MeV, $\frac{3}{2}^+$ (resonance state)] for the ^{12}C+^{13}C system. These states have the main components of the single-particle states, $p\frac{1}{2}$, $s\frac{1}{2}$, $d\frac{5}{2}$, and $d\frac{3}{2}$ of the valence nucleon in ^{12}N or ^{13}C, respectively.

In the previous papers [4,5,8,9] we have carried out the OCRC rotating molecular orbital (RMO) calculation for the ^{12}C+^{13}C system in detail but within the framework of three-channel OCRC (the $1p\frac{1}{2}$, $2s\frac{1}{2}$, and $1d\frac{5}{2}$ states) model. As a new feature we include in this report the resonance state of ^{13}C* (8.2 MeV, $\frac{3}{2}^+$) as well as that of ^{13}N* (7.9 MeV, $\frac{3}{2}^+$) in the calculation. They correspond to the $1d\frac{3}{2}$ single-particle states. Although their excitation energies are about 8 MeV, they have strong influence on the whole CRC schemes, as discussed in this paper, even at energies where the $1d\frac{3}{2}$ channels are closed.

We also take into account the inelastic transitions induced by the core-core interaction, which have been neglected in the OCRC calculations made so far [4,5,8,9]. The Coulomb part of this interaction causes the so-called effective charge for the dipole ($E1$) transition of the valence nucleon. When the target nucleus is very heavy and hence has big charge, this interaction mechanism dominates the transition related to the nuclear interaction. Recently Motobayashi et al. [10] have studied the dipole transition between the $1p\frac{1}{2}$ and $2s\frac{1}{2}$ states in ^{13}N with the inelastic scattering of the ^{13}N+^{208}Pb system at 78.1 MeV/u incident energy. They have observed large Coulomb-excitation cross sections. Such

strong dipole ($E1$) transitions have been reported also for the ^{14}O+^{208}Pb system by the same authors [10], and for the ^{11}Be+^{208}Pb system by Anne et al. [11] and Nakamura et al. [12]. The transition to the giant dipole resonance in ^{11}Li has been also extensively discussed by many authors [13,14]. In the case of light heavy-ion reactions at energies below the Coulomb barrier such dipole ($E1$) transition may dominate also the inelastic scattering, because the effects of the nuclear interaction is almost negligible at these energies. The very long tails of the wave functions of the $2s\frac{1}{2}$ states especially for the valence proton in ^{13}N (see Fig. 2) may give a possibility to enhance the dipole transition. We check these effects on the inelastic scattering ^{13}C(^{12}C, ^{12}C)^{13}C*($\frac{1}{2}^+$) and ^{13}N(^{12}C, ^{12}C)^{13}N*($\frac{1}{2}^+$).

So far, a lot of experimental data for the elastic and inelastic scattering and the fusion cross sections of the ^{12}C+^{13}C system have been accumulated [3,9,15–17,19], while concerning the ^{12}C+^{13}N system only elastic scattering data measured by Liénard et al. [2] are available. Thus, at first we make the OCRC analysis for the ^{12}C+^{13}C system to find optimum values of the parameters of the optical potential so that the calculation reproduces the experimental data measured by Voit et al. [9] for the angular distributions of the elastic and inelastic scattering ^{13}C(^{12}C, ^{12}C)^{13}C (gr., $\frac{1}{2}^-$; 3.09 MeV, $\frac{1}{2}^+$; 3.85 MeV, $\frac{5}{2}^+$) at energies 7.8, 8.3, 8.84, 9.88, 10.72, 11.52, 11.72, and 12.72 MeV of the center of mass. We also use the data of the fusion cross sections measured by Dasmahapata et al. [15] at energies below the Coulomb barrier.

We have performed the OCRC analysis for the ^{12}C+^{13}N system by using the parameters obtained by the calculation mentioned above. Then, we discuss the validity of our OCRC model with respect to the charge symmetric property for the ^{12}C+^{13}N and ^{12}C+^{13}C systems and the reaction mechanisms deduced from the OCRC analysis for both the systems. We pay special attention to the CRC effects which are expected to be very strong because of the effects of the hybridization [5,7], i.e., the mixing effects of the different parity single-particle states of the valence nucleon.

The fusion cross sections for the above systems should reflect the reaction mechanisms influenced by the valence nucleon. The additional nucleon to the ^{12}C+^{13}C system causes strong enhancement of the fusion cross sections of the ^{12}C+^{13}C system at energies below and near the Coulomb barrier, as found by many authors [15–17]. The role of the active nucleons in the enhancement of fusion cross sections in heavy-ion reactions at sub-barrier energies has been extensively discussed so far [18].

The reaction mechanism for the fusion is very interesting from the view point of the old question on nonobservation of the resonance phenomena in the ^{12}C+^{13}C system at energies below and near the Coulomb barrier [15–17,19], although the sharp and isolated resonances clearly exist in the ^{12}C+^{12}C system. These resonances have been found by Bromley and his collaborators [20] at first and also by many authors [21] later, and the resonance mechanism has been interpreted as due to the formation of di-nuclear molecular states of the ^{12}C+^{12}C system. Chua et al. [19] have investigated the dynamic motion of the valence nucleon in the
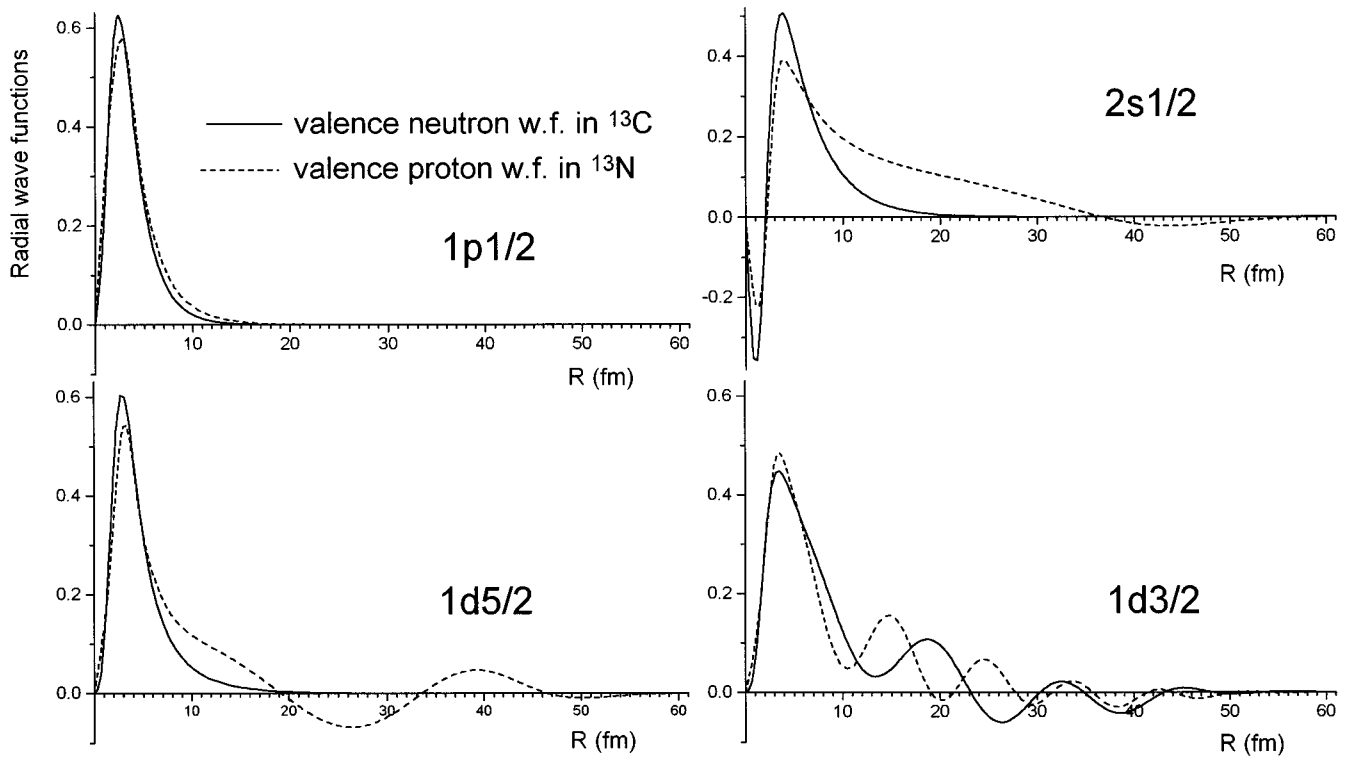
FIG. 2. Radial dependence of the valence-particle wave functions in ^{13}C or ^{3}N in the ground state $1p\frac{1}{2}$ and the excited states $2s\frac{1}{2}$, $1d\frac{5}{2}$, and $1d\frac{3}{2}$. The solid curves show the wave functions of the neutron in ^{13}C and the dashed curves those of the proton in ^{13}N.

^{12}C+^{13}C system, and suggested that the valence nucleon smears out the resonance phenomena observed in the system ^{12}C+^{12}C. However, the details of the reaction mechanisms have not yet been clarified explicitly. We discuss this problem in this report by analyzing the CRC mechanisms of the ^{12}C+^{13}C system in detail.

In Sec. II we explain briefly the OCRC theory employed in the analysis in this report. In Sec. III we show the result of the numerical analysis for the ^{12}C+^{13}N and ^{12}C+^{13}C systems, and discuss the reaction mechanisms for both the systems. The summary and the discussion with the use of the RMO model are given in Sec. IV.

II. OUTLINE OF THE OCRC ANALYSIS

In this paper we assume that the systems ^{12}C+^{13}N (or ^{12}C+^{13}C) consist of one valence nucleon in ^{13}N (or ^{13}C) and two ^{12}C nuclei. We restrict ourselves to the discussion in the framework of the channel wave functions concerned with the inelastic and transfer processes (core-exchange processes [3]) of the valence nucleon. The inelastic channels related to the rotational modes of the nucleus ^{12}C are not taken into account explicitly in the calculation. We assume that these effects are included in the optical potential used in the analysis.

We introduce here a new form of the derivation into our orthogonalized CRC (OCRC) formalism [5] *for the case of identical core nuclei*, and include the coupled discretized continuum channel (CDCC) method [22,23] in the frame of the OCRC theory in order to treat the single-particle *resonance states* of the valence nucleon in ^{13}C and ^{13}N. Hereafter, we explain our OCRC theory used here briefly, based

on the discussion given in Ref. [5].

The channel wave functions $\phi_i^{JM\Pi}(\hat{\mathbf{r}},\mathbf{R}C_1;C_2)$ are constructed from the wave function $Y_{L_i}(\hat{\mathbf{r}})$ of the relative motion in the eigenstate of the angular momentum L_i, the wave function $\varphi_{I_1}(\mathbf{R}C_1)$ of the nucleus, (valence nucleon+C_1) in the eigenstate of the angular momentum I_1 and the wave function $\varphi_{I_2}(C_2)$ of the nucleus C_2 in the eigenstate of the angular momentum I_2. The distance between the core C_1 and the valence nucleon is denoted by $\mathbf{R}$ and the relative distance between the two fragment nuclei by $\mathbf{r}$ (see Fig. 3). The angular parts of the $\mathbf{r}$ and $\mathbf{r}'$ are expressed by $\hat{\mathbf{r}}$ and $\hat{\mathbf{r}}'$, respectively. The suffix ''i'' denotes a set of quantum numbers needed to specify channel wave functions as well as a particular mass partition of the system. They are given by the equation,

$$\phi_i^{JM\Pi}(\hat{\mathbf{r}},\mathbf{R}C_1;C_2)=\{Y_{L_i}(\hat{\mathbf{r}})\otimes[\varphi_{I_1}(\mathbf{R}C_1)\otimes\varphi_{I_2}(C_2)]_I\}_{JM},$$
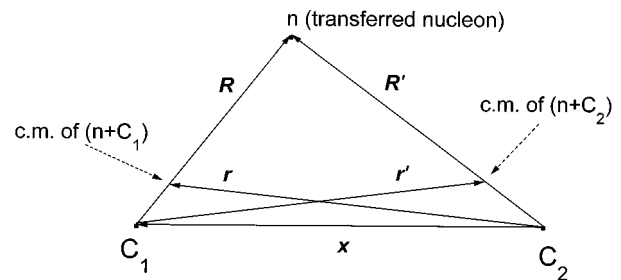(1)

FIG. 3. Definition of the coordinates used in the OCRC method.

TABLE I. Parameters of the potential $V_{nC}(R)$ between valence particle and core nucleus.

$$V_{nC}(R) = \frac{1+(-)^\pi}{2} \frac{V^+}{1+\exp[(R-R^+)/a^+]} + \frac{1-(-)^\pi}{2} \frac{V^-}{1+\exp[(R-R^-)/a^-]} + (\ell S)\frac{1}{R}\frac{d}{dR}\frac{V'}{1+\exp[(R-R')/a']} + V_{\text{Coul.}}(R_C)$$

with $R^+ = 2r_0^+ A^{1/3}$, $R^- = 2r_0^- A^{1/3}$, $R' = 2r_0' A^{1/3}$, and $R_C = 2r_C A^{1/3}$

	$\pi=-$			$\pi=+$			(ℓS)			
System	r_0^- (fm)	a^- (fm)	V^- (MeV)	r_0^+ (fm)	a^+ (fm)	V^+ (MeV)	r_0' (fm)	a' (fm)	V' (MeV)	r_C (fm)
$n+^{12}$C	1.16	0.705	-57.4	1.16	0.728	-73.62	1.16	0.705	-29.56	
$p+^{12}$C	1.193	0.700	-48.27	1.25	0.700	-59.39	1.25	0.700	-28.18	1.25

where J and Π are the angular momentum and the parity of the total system, respectively. The quantity M is the Z component of J in the laboratory frame. The wave function $\varphi_{I_1}(\mathbf{R}C_1)$ is expressed with the use of the fractional parentage coefficient (CFP) $\langle j\ell, I_C(nC_1)|\}I_1(C_1+n)\rangle$ as,

$$\varphi_{I_1}(\mathbf{R}C_1) = \sum \langle j\ell, I_C(nC_1)|\}I_1(C_1+n)\rangle \varphi_{j\ell}(\mathbf{R})\psi_{I_C}(C_1), \quad (2)$$

with the use of the wave function $\psi_{I_C}(C_1)$ of the core nucleus C_1 in the eigenstate of the angular momentum I_C and the wave function $\varphi_{j\ell}(\mathbf{R})$ of the valence nucleon with the angular momentum j and the orbital angular momentum ℓ. Since we take into account only the ground state (0^+) for the ^{12}C nucleus, the total angular momentum J is determined by the product of the angular momenta j and L_i.

The elastic and the inelastic transfer channels are automatically produced by the requirement of the symmetry property for the exchange of two identical core nuclei ($C_1 \equiv C_2$) [3]. Thus, the total wave function is expressed as

$$\Psi^{JM\Pi}(\tau) = \sum_i \{\phi_i^{JM\Pi}(\hat{\mathbf{r}}, \mathbf{R}C_1; C_2)\nu_i^{J\Pi}(r)/r$$
$$+ (-)^{N_C}\phi_i^{JM\Pi}(\hat{\mathbf{r}}', \mathbf{R}'C_2; C_1)\nu_i^{J\Pi}(r')/r'\}, \quad (3)$$

with

$$\tau = (\mathbf{r}, \mathbf{R}, C_1, C_2) = (\mathbf{r}', \mathbf{R}', C_2, C_1). \quad (4)$$

In the above equations the distances $\mathbf{r}'$ and $\mathbf{R}'$ are the coordinates to express the core-exchange channels (transfer channels) (see Fig. 3), and the symbol N_C denotes the number of nucleons in the core nucleus. Hereafter, we will drop the suffices J, Π, and M for the wave functions and other quantities, as far as there is no source of confusion.

We define the following new channel wave functions *in the whole space* τ as a linear combination of the wave functions of the direct and core-exchange channels;

$$|ir''\rangle = |ir'':D\rangle + (-)^{N_C}|ir'':E\rangle, \quad (5)$$

with

$$\langle\tau|ir'':D\rangle = \phi_i(\hat{\mathbf{r}}, \mathbf{R}C_1; C_2)\delta(r-r'')/r'', \quad (6)$$

$$\langle\tau|ir'':E\rangle = \phi_i(\hat{\mathbf{r}}', \mathbf{R}'C_2; C_1)\delta(r'-r'')/r''. \quad (7)$$

Then, the *orthogonal basis* $\{|kr\rangle\}$ are constructed from the above *nonorthogonal channel wave functions* as,

$$|kr\rangle = \sum_i \int dr''|ir''\rangle[N^{-1/2}(r'',r)]_{ik}, \quad (8)$$

where the overlap integral N is defined by the equation,

$$N_{ik}(r,r') = \langle ir|kr'\rangle. \quad (9)$$

By making use of the above *orthogonalized* channel wave functions, we have the following expression for the total wave function Ψ given in Eq. (3):

$$\Psi = \sum_i \int dr|ir\rangle u_i(r)/r. \quad (10)$$

The wave functions $u_i(r)$ in the above equation are related to the wave functions $\{\nu_k(r)\}$ defined by the nonorthogonal basis as,

$$u_i(r) = \sum_k \int dr'[N^{-1/2}(r,r')]_{ik}\nu_k(r'). \quad (11)$$

We assume that the effective Hamiltonian H_{eff} for the total system contains the interactions, $V_{nC}(\mathbf{R})$ between the valence nucleon and the core nucleus C_1, $V_{nC}(\mathbf{R}')$ between the valence nucleon and the other core nucleus $C_2(=C_1)$, and $V_{CC}(\mathbf{x})$ between the two core nuclei. The interaction V_{nC} generates the single-particle wave functions of the nucleon in ^{13}N or ^{13}C. The parameters of V_{nC} are determined so as to reproduce the separation energies and/or the resonance energies as well as their widths. The interaction V_{CC} is the optical potential between two core nuclei and the most important interaction to create the channel-diagonal parts $U_{ii}(r)$ of the direct interaction $U(r)$ [see Eq. (13)]. The parameters of V_{CC} are determined so as to reproduce the experimental data for the systems, ^{12}C+^{13}C and ^{12}C+^{13}N. This is discussed in detail in Sec. III.

In our previous studies [4,5,8,9] the inelastic transitions of the valence nucleon are generated only by the interaction

TABLE II. CFP values of single-particle states used in the calculations.

Nucleus	$1p\frac{1}{2}$	$2s\frac{1}{2}$	$1d\frac{5}{2}$	$1d\frac{3}{2}$
^{13}C	0.78	0.80	0.92	0.90
^{13}N	0.78	0.80	0.92	0.90

TABLE III. Parameters of the core-core optical potential $V_{CC}(\Pi j E_{c.m.}; r)$, where "$j$" specifies channel.

$$V_{CC}(\Pi j E_{c.m.}; r) = \frac{1-(-)^{\Pi}}{2} \frac{V^- + \hat{V}^- E_{c.m.}}{1+\exp[(r-1.42\times 2A^{1/3})/0.22]} + \frac{1+(-)^{\Pi}}{2} \frac{V^+ + \hat{V}^+ E_{c.m.}}{1+\exp[(r-1.25\times 2A^{1/3})/0.51]}$$

$$+ i W_j(E_{c.m.})\left\{ \frac{1-(-)^{\Pi}}{2} \frac{1}{1+\exp[(r-1.44\times 2A^{1/3})/1.03]} + \frac{1+(-)^{\Pi}}{2} \frac{1}{1+\exp[(r-1.32\times 2A^{1/3})/0.96]} \right\},$$

$$W_j(E_{c.m.}) = \begin{cases} -0.7(1-1/[1+\exp\{1.5487(E_{c.m.}-5.7754)\}]), & \text{for } j=1 \text{ (elastic channel)} \\ \left.\begin{matrix} -0.94-0.2\,E_{c.m.}, & \text{for } E_{c.m.}<9 \text{ MeV} \\ -2.74, & \text{for } 9\ \text{MeV}<E_{c.m.} \end{matrix}\right\} & \text{for } j\geq 2 \text{ (inelastic channel)}. \end{cases}$$

(unit of r; in fm, unit of energy; in MeV, $A=12$).

Π	$E_{c.m.}$ (MeV)	V^{Π} (MeV)	$\hat{V}^{\Pi}$ (MeV)
$-$	<6	-22.2	0.0
	>6	-27.0	0.8
$+$	<7.8	-19.76	0.0
	>8.3	-24.0	0.8

V_{nC}, and not by the interaction V_{CC}, because the mass of the valence nucleon is regarded to be as small as negligible compared to that of the core nucleus. However, the Coulomb interaction contained in the V_{CC} increases with increasing masses of the core nuclei. Thus, the effects of the Coulomb part of the interaction V_{CC} may not necessarily be negligible in the case where it causes dipole ($E1$) transition [10–14] between two orbits of the valence nucleon. We estimate this effect exactly.

The single-particle states $d\frac{3}{2}$ in ^{13}C, and $s\frac{1}{2}$, $d\frac{5}{2}$, and $d\frac{3}{2}$ in ^{13}N adopted in this calculation are resonance states, and the wave functions do not converge in the asymptotic region. Thus, the direct and the transfer interactions (U and K^t) are not determined definitely. In order to avoid this situation, we employ the coupled discretized continuum channels (CDCC) method developed by Austern, Rawitcher, Kamimura, Kawai, Sakuragi, and their collaborators [22,23], that is, we use, instead of the resonance wave functions, the wave packets $\varphi_{n\ell}(R;E_r)$ defined by the following equations:

$$\varphi_{j\ell}(\mathbf{R};E_r) = \frac{1}{N^{\text{norm}}} \int_{-\infty}^{\infty} dE \frac{\text{real}[w_{j\ell}(\mathbf{R};E)]}{\sqrt{(E-E_r)^2+(\Gamma/2)^2}}, \quad (12)$$

where E_r and Γ are the resonance energy and its width, respectively, and $w_{j\ell}(\mathbf{R};E)$ is the scattering wave function obtained by the potential V_{nC} at energy E. The above wave packet is normalized by the quantity N^{norm}.

We obtain the OCRC equation for the radial wave functions $u_i(r)$ ($i=1,..,n$), by inserting Eq. (10) into the equation $(E-H_{\text{eff}})\Psi=0$. This equation contains two *nonlocal* terms $K^t(=[K^t_{ij}])$ and $\Delta M(=[\Delta M_{ij}])$ as the effective transfer interactions [5]. The nonlocality reflects the recoil effects coming from the particle transfers. These terms make it very difficult to solve the OCRC equation numerically. In order to overcome these difficulties, we make the following assumptions for the K^t and ΔM.

(1) We neglect the term $\Delta M(=O[(I-N)^2])$ (I: unit operator), because we discuss the reaction mechanisms induced by the valence nucleon *in the peripheral region*, where the quantity $(I-N)$ is relatively small, as discussed in Ref. [5].

(2) The nonlocal transfer interaction K^t is approximated by a local form. This is good approximation at low energies, as discussed in Refs. [24] and [25]. As shown in Ref. [24] for the analysis of the ^{36}S + ^{37}Cl system, the OCRC result with this approximation agrees well with the result obtained by using the full finite-range CRC code, FRESCO made by Thompson [26].

Thus, we have the radial OCRC equations which contains spatially local interactions only,

$$\{E-[t+R(r)+K^t(r)+U(r)]\}\mathbf{u}(r)=0, \quad (13)$$

where $\mathbf{u}(r)$ is the vector consisting of the radial wave functions $u_i(r)$ ($i=1,...,n$) for the relative motion, and the matrices t, R, and U represent the kinetic energy operator $[-\delta_{ij}(\hbar^2/2\mu)d^2/dr^2]$, the centrifugal potential $[(\hbar^2/2\mu)L^2_{ij}/r^2]$, and the direct interactions $[U_{ij}(r)]$, respectively. The direct interaction U is obtained by the folding procedure for the interactions V_{nC} and V_{CC} with the single-particle wave functions, and is responsible for the direct elastic and inelastic transitions (direct processes) of the valence particle, i.e., the transitions between the basis functions $|ir:D\rangle$ and $|jr':D\rangle$ (or between $|ir:E\rangle$ and $|jr':E\rangle$) of the same mass partition. The transfer interaction K' is expressed as

$$K^t = \frac{1}{2\sqrt{N}}(F+F^T)\frac{1}{\sqrt{N}}, \quad (14)$$

where F and F^T are the *transfer interaction used in the distorted wave Born approximation and its transposed operator*, respectively. The interaction F causes the nucleon elastic or inelastic transfer between the nonorthogonal basis functions $|ir:D\rangle$ and $|jr':E\rangle$. As found in the above equation, the transfer interaction K^t is the *symmetric operator* $[K^t=(K^t)^T]$ *consisting of the nonsymmetric operators F and F^T, and it is modified by the overlap integral N*. It should be noticed that the K^t contains neither the kinetic energy operator t nor the total energy E unlike the transfer interaction *used in the conventional* CRC *theory* [26]. In order to obtain

the scattering amplitudes and the cross sections of the elastic and inelastic scattering, we solve Eq. (13) under an appropriate boundary condition.

Molecular orbital states in this paper (rotating molecular orbital; RMO) are defined [5] as states which diagonalize all the interactions $[R(r)+K^t(r)+U(r)]$ contained in Eq. (15). Namely the RMO states are expressed as

$$\Phi_p(r)=\sum_i |ir\rangle A_{ip}(r), \qquad (15)$$

with the use of the transformation matrix $A(r)$ for the following diagonalization:

$$\{A^{-1}(r)[R(r)+K'(r)+U(r)]A(r)\}_{qp}=\delta_{qp}\mathscr{V}_p(r). \qquad (16)$$

The RMO states depend on the total angular momentum J, because the rotational operator $R(r)$ of the relative motion is included in the above equation. The quantity $\mathscr{V}_p(r)$ is the adiabatic potential corresponding to RMO state "p."

In this paper we pay special attention to the fusion cross sections, particularly at energies below and near the Coulomb barrier, which is expressed as

$$\sigma_{\text{fus}}\equiv\sigma_{\text{abs}}-\sum_{j(=\text{incident})}\sigma_j(\text{reac})$$

$$=\sum_{i(=\text{incident})}\frac{i\pi}{k_i^2}\sum_{J\Pi}(2J+1)$$

$$\times\sum_{kl}\langle u_{ki}^{J\Pi(+)},(U-U^\dagger)_{kl}u_{ii}^{J\Pi(+)}\rangle, \qquad (17)$$

where σ_{abs} is the total absorption cross section and $\sigma_j(\text{reac})$ the angle-integrated reaction cross section of channel j. The wave functions $u_{ki}^{J\Pi}$ ($k=1,\ldots,n$) are the solutions of Eq. (13) obtained by the outgoing boundary condition with the incident wave from channel i and k_i is the wave number of the channel i. The detail of the derivation of the above equation is given in Ref. [4].

III. ANALYSIS OF THE EXPERIMENTAL DATA

At first we analyze the system ^{12}C+^{13}C with the OCRC method explained in the previous section, since we have numerous experimental data for the elastic and inelastic scattering for this system. Then, we analyze the data of the elastic scattering of ^{13}N on ^{12}C measured by Liénard et al. [2].

We choose the interaction V_{nC} which reproduces the single-particle states of the $p\frac{1}{2}$, $s\frac{1}{2}$, $d\frac{5}{2}$, and $d\frac{3}{2}$ with the separation/resonance energies of the valence nucleon for the states $\frac{1}{2}^-$(ground), $\frac{1}{2}^+$(3.086 MeV), $\frac{5}{2}^+$(3.854 MeV), and $\frac{3}{2}^+$(8.2 MeV) of the ^{13}C nucleus, respectively, or for the states $\frac{1}{2}^-$(ground), $\frac{1}{2}^+$(2.365 MeV), $\frac{5}{2}^+$(3.547 MeV), and $\frac{3}{2}^+$(7.9 MeV) of the ^{13}N nucleus, respectively. The parameters obtained are listed in Table I for both the systems. The radial dependence of the single-particle wave functions (or the wave packets) for the respective states are shown in Fig. 2. We assume for these states the single particle CFP values given in Table II. They are close to the values obtained by the shell model calculation [27]. By using the quantities
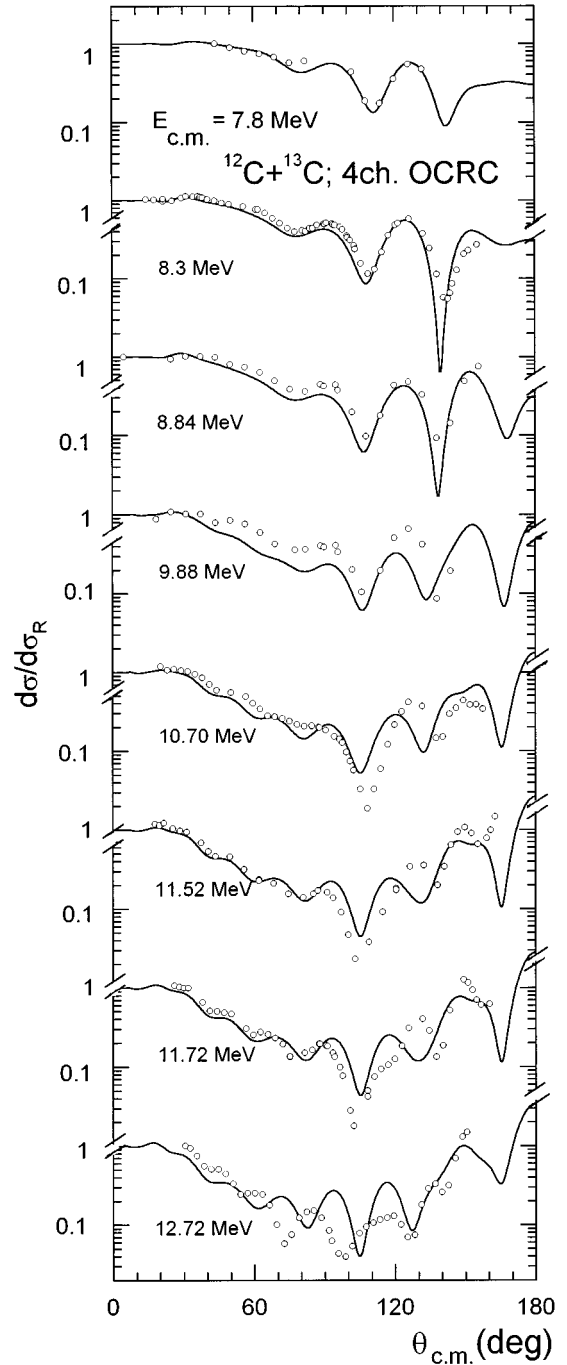

FIG. 4. Angular distributions for the elastic scattering of ^{13}C on ^{12}C at energies $E_{\text{c.m.}}=7.8$, 8.3, 8.84, 9.88, 10.70, 11.52. 11.72, and 12.72 MeV. The solid curves show the four-channel OCRC calculations and the circles the experimental data from Ref. [9].

mentioned above and the single-particle wave functions generated by the V_{nC}, we get the effective interactions U for the direct processes (direct elastic and inelastic transitions) and the effective interactions K^t for the transfer processes (the elastic and inelastic transfer processes).

A. Analysis of the ^{12}C+^{13}C system

We make the OCRC calculation and the parameter search on the optical potential V_{CC} so as to reproduce the experimental data of the angular distributions of ^{13}C(^{12}C, ^{12}C)
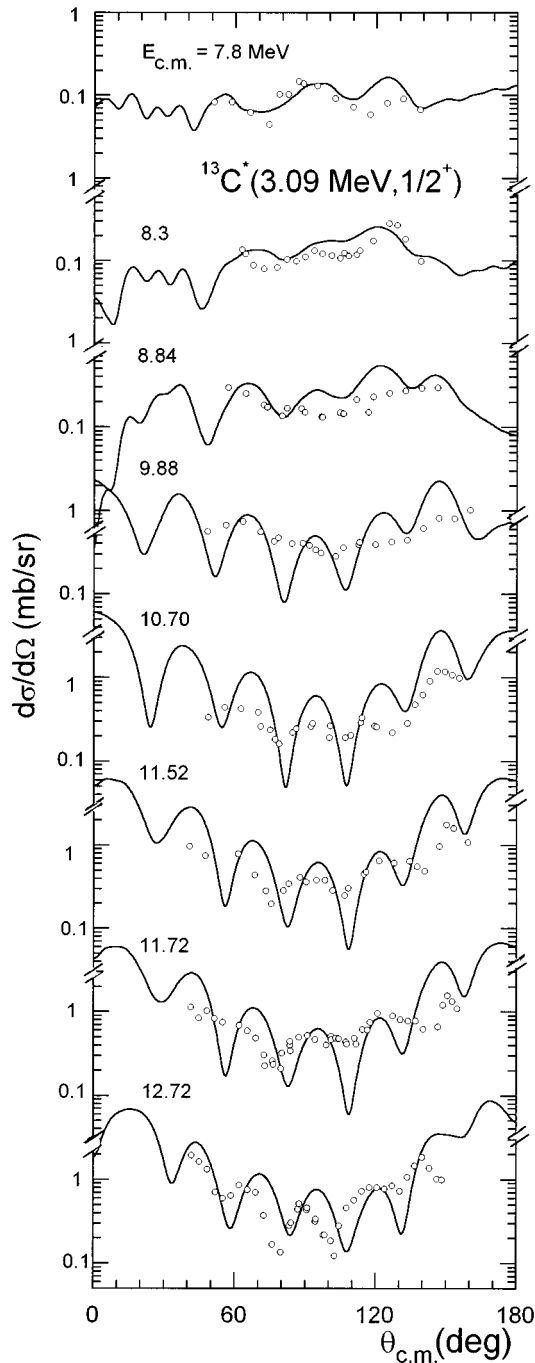
FIG. 5. As Fig. 4 for the inelastic scattering $^{13}C(^{12}C, {}^{12}C)^{13}C^*$ (3.09 MeV, $\frac{1}{2}^+$).

FIG. 6. As Fig. 4 for the inelastic scattering $^{13}C(^{12}C, {}^{12}C)^{13}C^*$ (3.85 MeV $\frac{5}{2}^-$).

^{13}C(gr $\frac{1}{2}^-$; 3.09 MeV, $\frac{1}{2}^+$; 3.85 MeV, $\frac{5}{2}^+$) at $E_{c.m.}=7.8$, 8.3, 8.84, 9.88, 10.70, 11.52, 11.72, and 12.72 MeV, which were measured by Voit *et al.* [9]. In order to do this, we use an automatic parameter-search program code together with the manual parameter search. We allow the parameters to depend on the total parity Π of the system and on channels of the elastic and inelastic scattering.

At first, however, we tried to find a parameter set which depends neither on the channels nor on the total parity. In this case any effort failed in reproducing the data of the inelastic scattering, that is, it is very difficult to represent the phases of peaks and valleys as observed in the experimental data, especially for the inelastic scattering $^{13}C(^{12}C,$
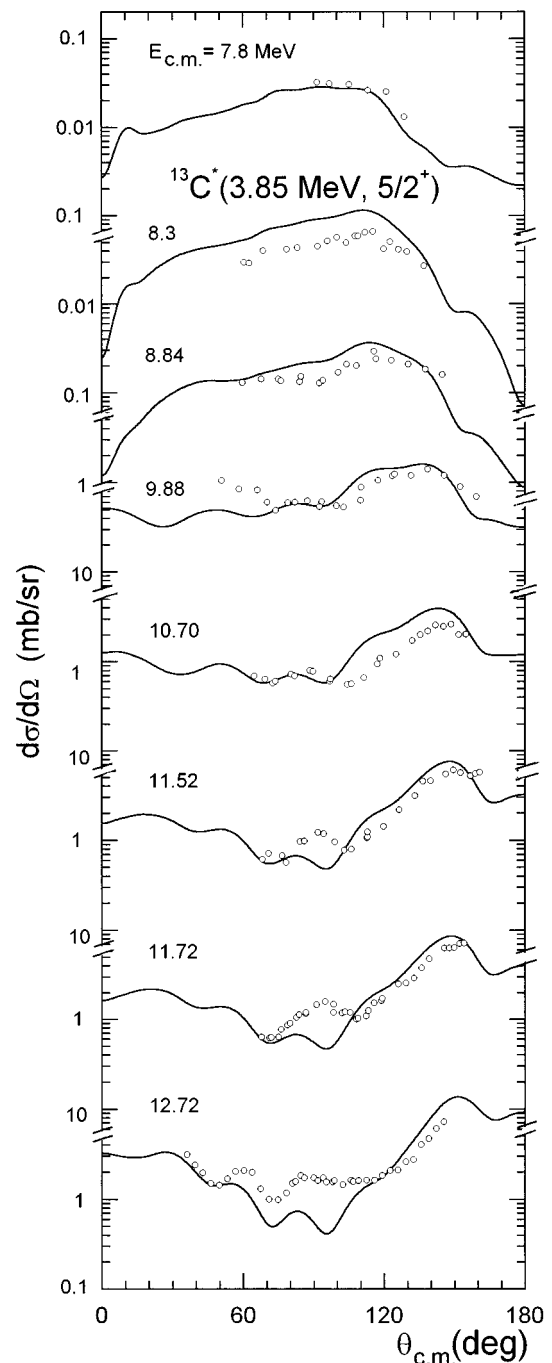
$^{12}C)^{13}C^*(\frac{1}{2}^+)$. Furthermore, these cross sections, in particular of the inelastic scattering to $^{13}C^*(\frac{1}{2}^+)$ are overestimated at any energies, if we adjust the parameters so as to reproduce the data of the elastic scattering at forward angles. This means that the depth of the imaginary potential is too weak to reproduce such smaller magnitudes as observed in the experimental data of the inelastic cross sections. On the other hand, if we employ deeper imaginary potential to fit to the inelastic scattering data, the absorption in the elastic channel becomes too strong, and the shoulder of the angular distribution at forward angles much decreases.
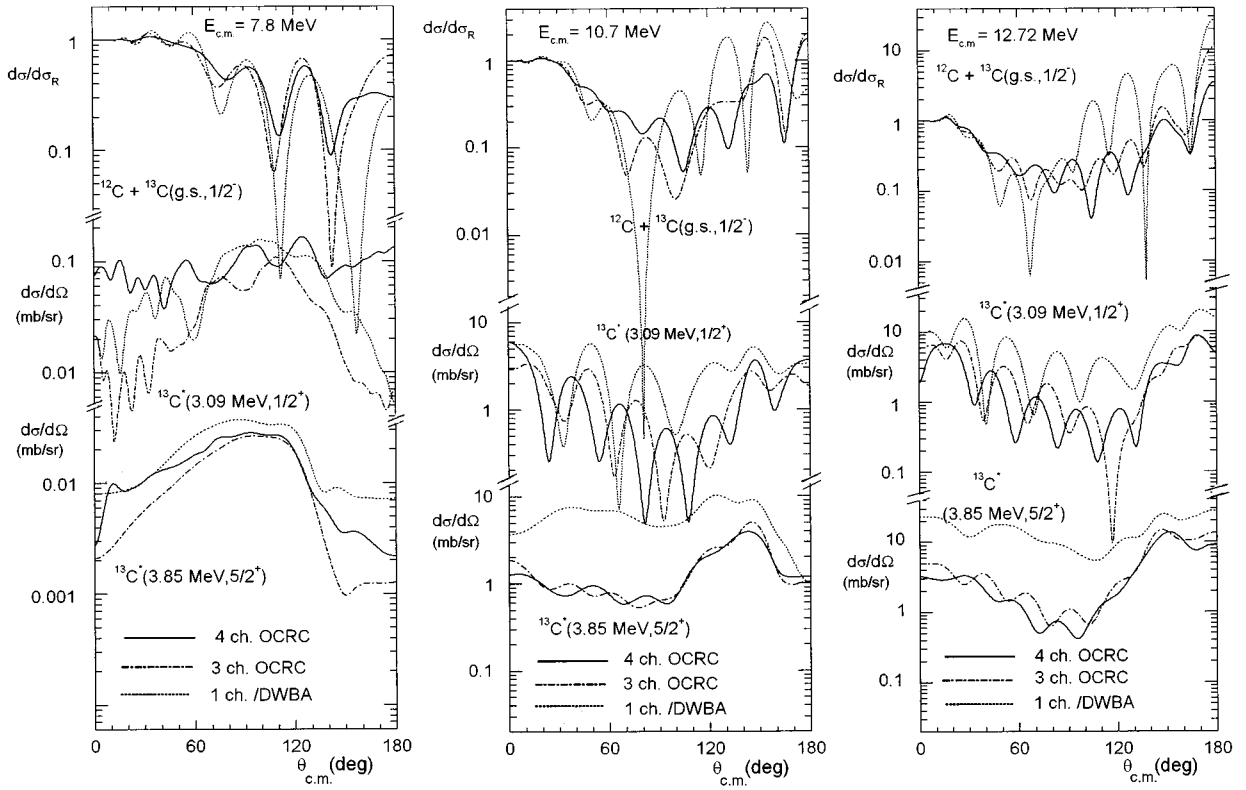
FIG. 7. Angular distributions of the elastic and the inelastic scattering ^{13}C(^{12}C, ^{12}C)^{13}C(*) (gr., $\frac{1}{2}$; 3.09 MeV, $\frac{1}{2}^{+}$; 3.85 MeV, $\frac{5}{2}^{+}$) at energies $E_{\text{c.m.}} = 7.8$, 10.7, and 12.72 MeV. The solid curves are the results of the four-channel OCRC calculations with the states $1p\frac{1}{2}$, $2s\frac{1}{2}$, $1d\frac{5}{2}$, and $1d\frac{3}{2}$, and the dot-dashed curves those of the three-channel OCRC calculations with the states $1p\frac{1}{2}$, $1s\frac{1}{2}$, and $1d\frac{5}{2}$. The dotted curves show the one-channel/DWBA calculations (see the text.).

The use of the *potential, the real part of which depends on the total parity of the system*, improves dramatically the phase relation mentioned above at all the energies. Namely, we use larger radius parameter for the real part in negative-parity states than in positive-parity states and smaller diffuseness parameter in negative-parity states as listed in Table III. Such parity dependence may be caused by incomplete space truncation of the channel basis functions employed here. Probably the core excitation channels as well as the breakup channels may contribute to the parity dependence of the optical potential.

The conflict mentioned above between the magnitudes of the elastic scattering cross sections and those of the inelastic scattering cross sections is almost fully resolved, if we employ *channel-dependent imaginary potential*, i.e., weaker imaginary depth for the elastic channel than for the inelastic channels. The data of the fusion cross sections [15] at energies below the Coulomb barrier are reproduced also by a very week imaginary potential for the elastic channel. Then, we get generally good agreement of the calculation with the experimental data, as found in Figs. 4, 5, and 6, not only for the angular distributions of the elastic and inelastic cross sections but also for the fusion cross sections below the Coulomb barrier [see Fig. 17(a)]. Only at $E_{\text{c.m.}} = 9.88$ MeV the calculation of the angular distributions of the elastic scattering fairly deviates from the experimental data. This difficulty is also found in the analysis with the optical potential by Liénard *et al.* [2]. One of the possible explanations is an

appearance of resonance phenomena at this energy or the experimental error bars are underestimated.

The cause of the channel-dependent imaginary potential may be due to the breakup processes of the valence nucleon and the fusion processes. This will be discussed in Sec. IV.

We test the CRC effects by comparing the above OCRC results with the calculation where the coupling interactions ΔH_{ik} between different channels are considered as perturbations. Namely, the elastic scattering amplitudes are calculated within the framework of the complete elastic channel, while the inelastic scattering amplitudes are calculated by the procedure of the distorted wave Born approximation (DWBA), where the distorted waves $u_i^{(0)}(r)$ are generated by switching off the coupling interactions and the overlap integrals *except those for the elastic transfer*. As shown in Fig. 7, the OCRC results are very different from the DWBA results. This strong coupling feature comes from the channel mixings, especially from those called the hybridization, i.e., the mixings between different parity single-particle states of the p and d orbits. This has been discussed in detail in Refs. [4], [5], [8], [9], where we have made the three-channel OCRC calculation with the $p\frac{1}{2}$, $s\frac{1}{2}$, and $d\frac{5}{2}$ states.

The new feature, the introduction of the $d\frac{3}{2}$ channel into the OCRC calculation in this paper affects strongly the CRC scheme, as seen from the comparison of the three-channel calculation with the four-channel calculation in Fig. 7. The inclusion of the $d\frac{3}{2}$ channel causes the shifts for the phases of

the diffraction patterns observed in the angular distributions of the elastic and $\frac{1}{2}^+$-inelastic scattering. As mentioned before, the $d\frac{3}{2}$ channel gets to be closed at energies lower than $E_{\text{c.m.}}=8.2$ MeV. Nevertheless, the influence of the closed channel on the CRC scheme is still important even at such energies. The detailed discussion on these effects is given in Sec. III C.

B. Analysis of the $^{12}\text{C}+^{13}\text{N}$ system

Angular distributions of the elastic scattering for the $^{12}\text{C}+^{13}\text{N}$ system have been measured at $E_{\text{c.m.}}=7.824$, 9.6, and 14.16 MeV [2], however, the data for the inelastic scattering and any other reactions have not been obtained. Therefore, we can not perform, in the same way as in the case of $^{12}\text{C}+^{13}\text{C}$ system, optical-potential parameter search for the $^{12}\text{C}+^{13}\text{N}$ system. Thus, we attempt to apply the *optical potential obtained in the analysis of the $^{12}\text{C}+^{13}\text{C}$ system* directly to the charge symmetric $^{12}\text{C}+^{13}\text{N}$ system.

In Fig. 8 the four-channel OCRC calculations are compared with the experimental data. We see that the OCRC calculations reproduce the data of the elastic scattering fairly well especially at forward angles, without any modification of the optical potential parameters obtained in the analysis of the $^{12}\text{C}+^{13}\text{C}$ system. However, the cross sections are short of enhancement at backward angles, a little bit at $E_{\text{c.m.}}=7.824$ and 9.6 MeV and clearly at $E_{\text{c.m.}}=14.16$ MeV.

To improve this, we try the OCRC calculation with weaker imaginary potential by a factor $\frac{1}{5}$, as made by Liénard *et al.* [2] in their one-channel analysis. As shown in Fig. 9, the backward cross sections of the elastic scattering are enhanced fairly well, while the agreement of the calculation with the data clearly deteriorates at forward angles where the *elastic-scattering* cross sections should be originated, at distances around or larger than the grazing distance, mainly from the optical potential. From this result we can hardly draw a conclusion that the depth of imaginary potential for the $^{12}\text{C}+^{13}\text{N}$ system *should* be three-five times smaller than for the $^{12}\text{C}+^{13}\text{C}$ system. Instead we prefer the use of the same imaginary potential for both the systems $^{12}\text{C}+^{13}\text{N}$ and $^{12}\text{C}+^{13}\text{C}$. In the case of the $^{12}\text{C}+^{13}\text{C}$ system the same test as the above gives larger deviation of the calculations from the experimental data than in the case of the $^{12}\text{C}+^{13}\text{N}$ system, as seen in Fig. 10. Hence, the potential depth is better determined for the case of the $^{12}\text{C}+^{13}\text{C}$ system.

Although the CRC effects in the $^{12}\text{C}+^{13}\text{N}$ system are comparably weaker than those in the $^{12}\text{C}+^{13}\text{C}$ system, the effects themselves are still strong as seen in Fig. 11. The details of the CRC effects are discussed in the following Sec. III C.

The single-particle wave functions of the proton in ^{13}N have long tails except for the $p\frac{1}{2}$ ground state, and are very different from those of the neutron in ^{13}C as shown in Fig. 2. Reflecting this, the cross sections of the inelastic scattering are larger than those for the $^{12}\text{C}+^{13}\text{C}$ system generally. However, it should be noticed that this fact does not mean stronger CRC effects in the $^{12}\text{C}+^{13}\text{N}$ system than in the $^{12}\text{C}+^{13}\text{C}$ system. This issue will be discussed in Sec. IV from the view point of the molecular-orbital picture of the valence nucleon.
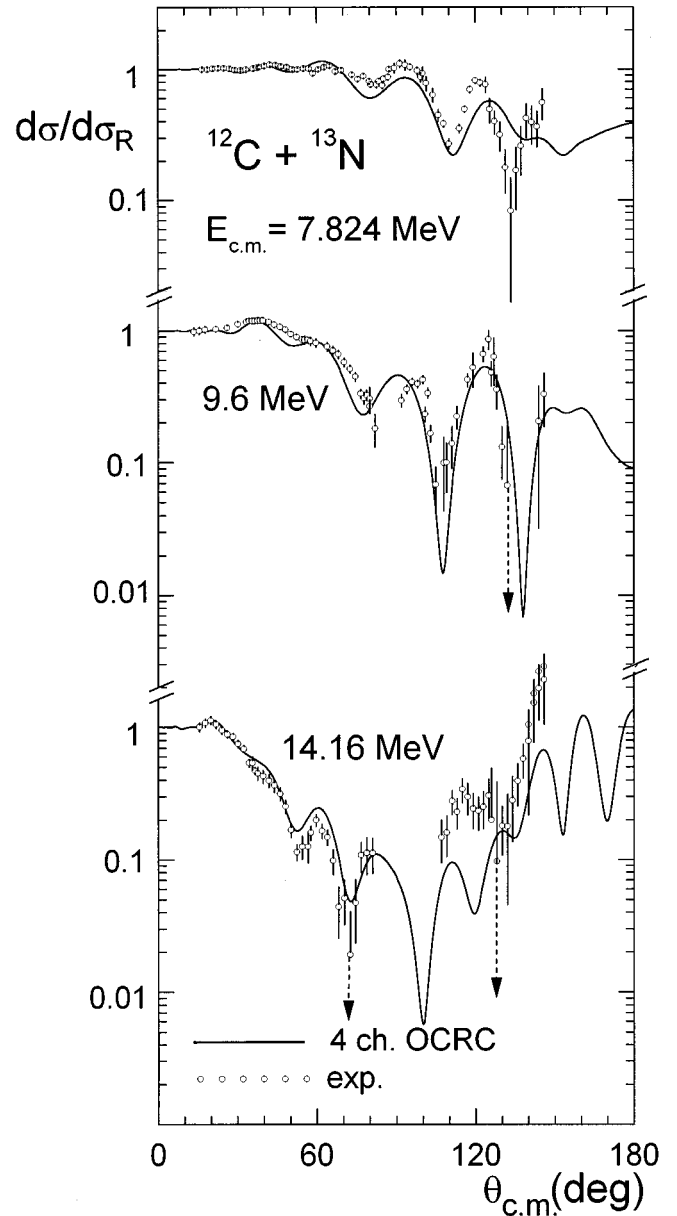

FIG. 8. Angular distributions of the elastic scattering of ^{13}N on ^{12}C at energies $E_{\text{c.m.}}=7.824$, 9.6, and 14.16 MeV. The solid curves show the four-channel OCRC calculations and the circles the experimental data from Ref. [2].

C. CRC effects of the coupling interactions of the $^{12}\text{C}+^{13}\text{C}$ and $^{12}\text{C}+^{13}\text{N}$ systems

The strong CRC effects, which have been observed in the differential cross sections of the elastic and inelastic scattering for the $^{12}\text{C}+^{13}\text{C}$ and $^{12}\text{C}+^{13}\text{N}$ systems, are discussed in Secs. III A and III B. These effects are so strong, especially at the total angular momenta lower than the grazing angular momentum, that the following distorted-wave Born (DWB) series (expansion in power series of the coupling interactions ΔH) of the T matrix $\{T_{ik}\}$ diverges

$$T_{ik}=T_i^{(0)}\delta_{ik}+\sum_{n=0}^{\infty}\langle u_i^{(0)},(\Delta H(g^{(0)}\Delta H)^n)_{ik}u_k^{(0)}\rangle, \quad (18)$$

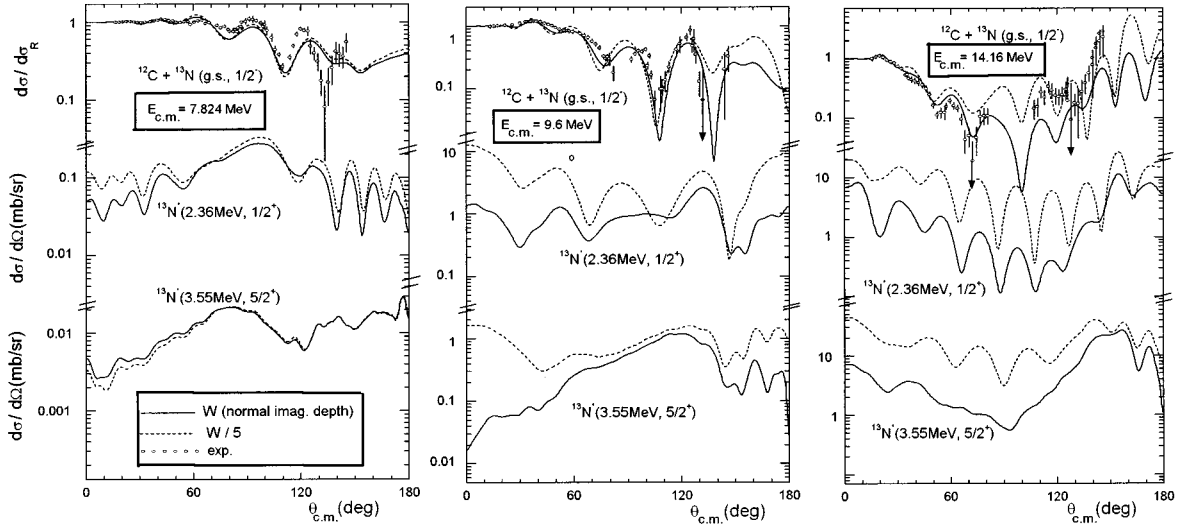FIG. 9. Angular distributions of the elastic and inelastic scattering ^{13}N(^{12}C, ^{12}C)^{13}N(*) (gr., $\frac{1}{2}$; 2.36 MeV, $\frac{1}{2}^+$; 3.55 MeV, $\frac{5}{2}^+$) at energies $E_{c.m.}=7.824$, 9.6, and 14.16 MeV. The dashed curves show the OCRC calculations obtained by the core-core optical potential with five times weaker *imaginary depth* than the standard one, while the solid curves the OCRC calculations with the use of the standard optical potential given in Table III. They are compared to the experimental data [2] shown by the circles.

where ΔH and $u^{(0)}$ are the coupling interactions and the distorted waves defined in Sec. III A, respectively. The quantity $g^{(0)}$ is Green's function of the Hamiltonian for the no-coupling system. With increasing angular momentum, however, the OCRC scattering amplitudes properly converge to those of the one-step distorted-wave Born approximation (DWBA) calculation. One of the criteria to see the extent of the CRC effects of the coupling interactions is to test the convergent properties of the DWB expansion (18).

Thus, we multiply a factor λ into the coupling interactions ΔH and then evaluate the critical value λ_c which gives the limit of the convergence of the DWB series. Therefore, the smaller is the value of λ_c, the stronger are the CRC effects. If λ_c is larger than unity, the DWB series with the normal strength ($\lambda=1$) of the coupling interactions converges.

We test this for both the systems ^{12}C+^{13}C and ^{12}C+^{13}N as shown in Fig. 12, by choosing the total angular momenta $J^{\Pi}=\frac{13}{2}^+$ and $\frac{21}{2}^+$, the former of J^{Π} corresponds to the grazing angular momentum at about $E_{c.m.}=8$ MeV for the ^{12}C+^{13}C system. In the case of the lower total angular momentum ($J^{\Pi}=\frac{13}{2}^+$) the DWB series for both the systems diverge at all the energies. In order to get the convergence, we need to reduce the strength of the coupling interactions by about 30%.

In the case of the higher total angular momentum ($J^{\Pi}=\frac{21}{2}^+$), however, the DWB series converges fast at lower energies especially for the ^{12}C+^{13}N system. This is because the centrifugal potentials with higher partial waves prevent the incident waves to approach the region where the coupling interactions are so strong as to cause the multistep processes, as seen in Fig. 12. In spite of this, in the case that the incident energy is a little bit lower than the potential barrier including the centrifugal potential as seen for the ^{12}C+^{13}C system at $E_{c.m.}=12$ MeV in Fig. 12, the DWB series diverges, indicating that the CRC effects are strong already at the distances fairly far from the grazing distance.

Generally the CRC *effects are stronger in the* ^{12}C+^{13}C *system than in the* ^{12}C+^{13}N *system as shown in Fig. 12.* The

same effects are also observed in the calculation of the nucleon molecular orbitals of the covalent molecule, that is, the concentration of the nucleon density at the center of the axis joining the centers of the two core ^{12}C nuclei is higher than in the ^{12}C+^{13}N system. This discussion will be given in Sec. IV in more detail.

D. Roles of the $d\frac{3}{2}$ resonance-state channel in the CRC scheme and the hybridization phenomena between the p and d single-particle orbits

By dropping the $d\frac{3}{2}$ resonance-state channel, we make the same test as in the previous section III C but with the use of three channels ($p\frac{1}{2}$, $s\frac{1}{2}$, and $d\frac{5}{2}$). As observed in Fig. 12, the value of λ_c is generally larger than that obtained in the four-channel OCRC calculation especially at lower energies, showing that the CRC effects in the four-channel calculation are stronger than in the three-channel calculation. Namely, the $d\frac{3}{2}$ channel enhances the CRC effects, although this channel is completely closed at these energies.

The coupling interactions consists of two parts, i.e. the transfer and direct processes parts [see Eq. (13)]. To see the CRC effects of the respective interactions separately, we made OCRC calculation only with the transfer interactions K^t or only with the direct interactions U also by introducing the factor λ_c mentioned in Sec. III C. In Fig. 13 we show three curves of λ_c for the respective systems ^{12}C+^{13}C and ^{12}C+^{13}N as functions of the energy. They correspond to the above two kinds of the four-channel OCRC calculations and to the four-channel OCRC calculation with the full interactions, respectively. Generally, as seen there, the transfer coupling interactions does not cause the divergence with the normal coupling strength ($\lambda=1$), while the direct interactions causes the divergence that the CRC effects, they are almost the same as those in the calculation with the full interactions especially in the ^{12}C+^{13}N system.

In the OCRC calculation with the use of the three channels, i.e., with dropping the $d\frac{3}{2}$ channel, however, the situa-

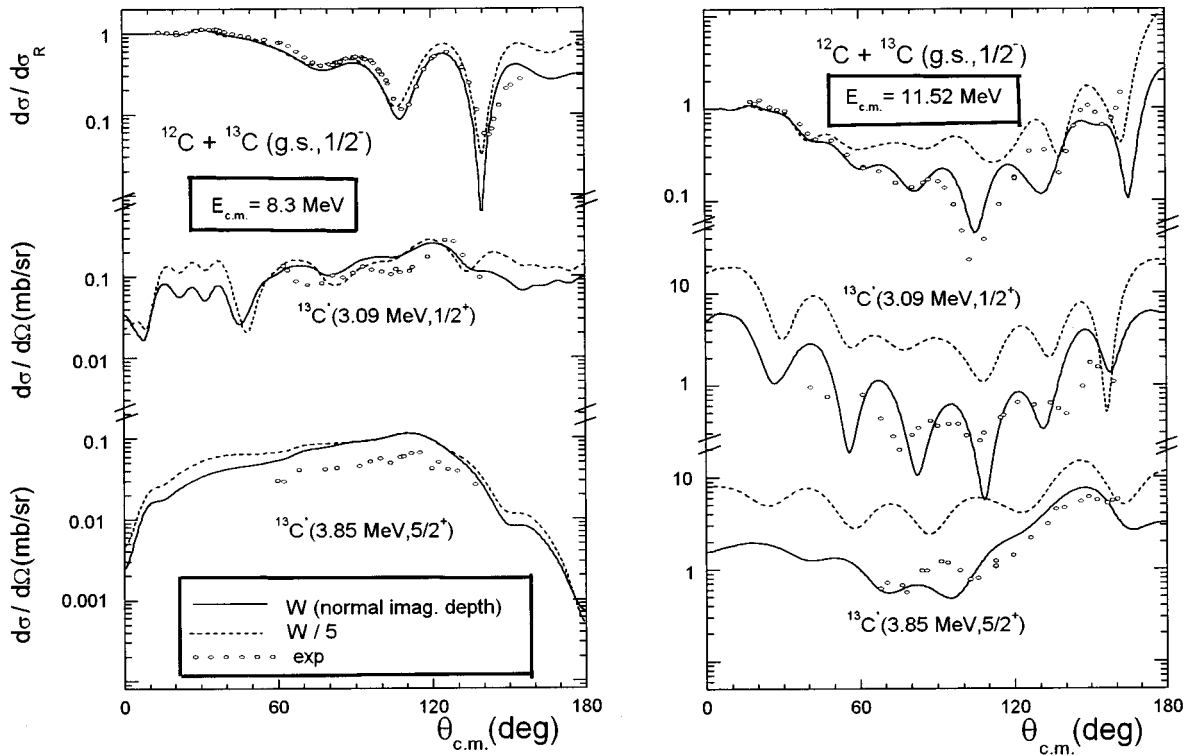FIG. 10. As Fig. 9 for the angular distributions of the elastic and the inelastic scattering $^{13}C(^{12}C, \, ^{12}C)^{13}C(*)$ (gr., $\frac{1}{2}^-$; 3.09 MeV, $\frac{1}{2}^+$; 3.85 MeV, $\frac{5}{2}^+$) at energies $E_{c.m.} = 8.3$ and 11.52 MeV.
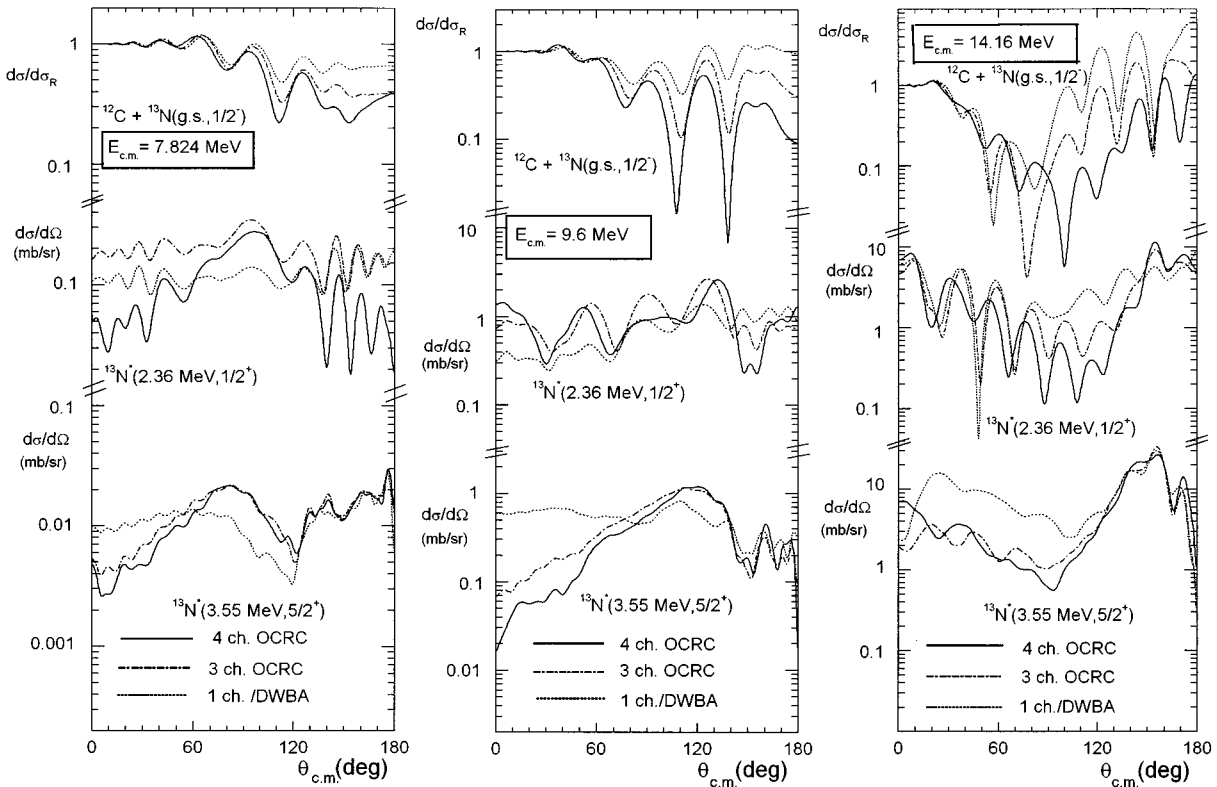

FIG. 11. As Fig. 7 for the elastic and inelastic scattering $^{13}N(^{12}C, \, ^{12}C)^{13}N(*)$ (gr., $\frac{1}{2}^-$; 2.36 MeV, $\frac{1}{2}^+$; 3.55 MeV, $\frac{5}{2}^+$) at energies $E_{c.m.} = 7.824$, 9.6, and 14.16 MeV.
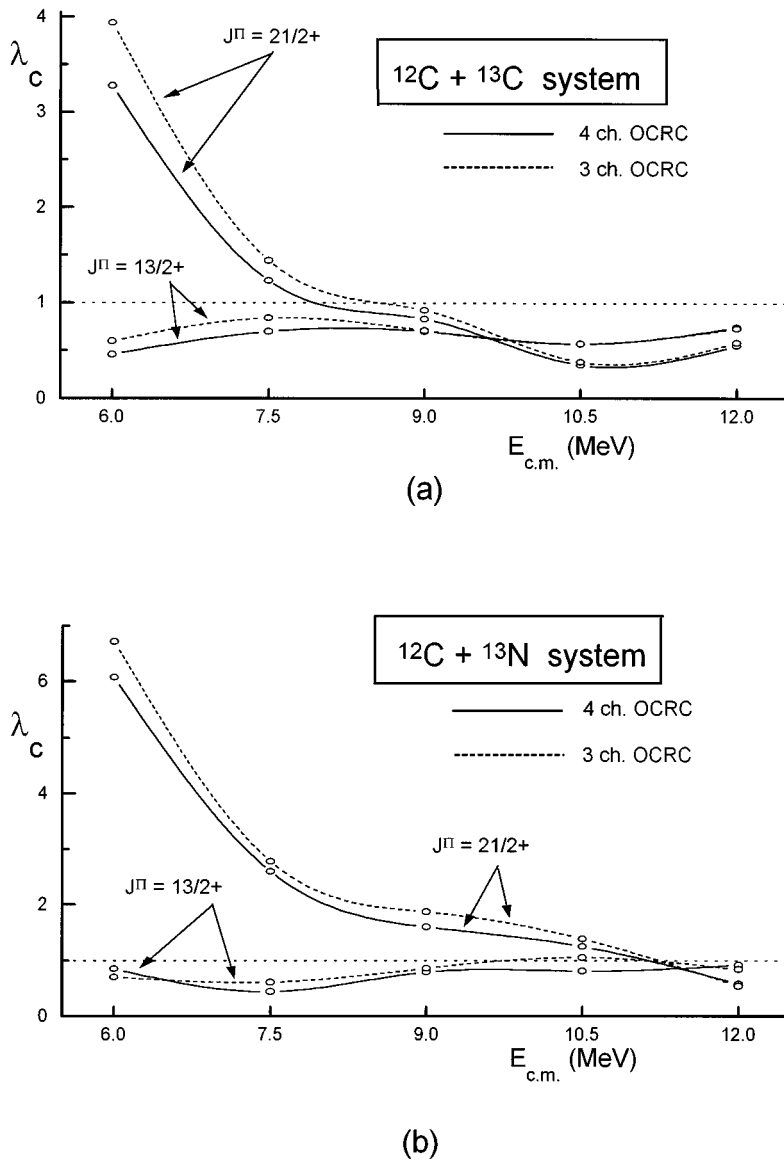
(a)

(b)

FIG. 12. Test of convergence of the distorted wave Born series. The critical values λ_c of the multiplication factor (see text.) into the coupling interactions are shown as functions of the energy, (a) for the ^{12}C+^{13}C system and (b) for ^{12}C +^{13}N system in the states of the total angular momentum $J^{\Pi}=\frac{13}{2}^+$ and $\frac{21}{2}^+$. The solid curves show the four-channel OCRC calculations and the dashed curves the three-channel OCRC calculations. Generally the values of λ_c for the four-channel CRC scheme are smaller than those for the three-channel CRC scheme, indicating that the CRC effects are stronger in the former than in the latter.

tion is somewhat different. Namely, when only direct coupling interactions are used, the OCRC effects of the three-channel calculation are fairly weaker than those of the four-channel calculation especially in the ^{12}C+^{13}N system and the DWB series of the three-channel calculation tends to converge with the normal coupling strength ($\lambda=1$), as seen in Fig. 14. On the other hand, when only the transfer coupling interactions are used, the CRC effects for both, the three-channel and the four-channel calculations are similar to each other. This means that the *direct coupling interactions between the $d\frac{3}{2}$ and the other channels cause the strong* CRC *effects*.

Of these direct coupling interactions the interaction between the ground state $p\frac{1}{2}$ and the $d\frac{3}{2}$ channels play a very important role in the formation of the strong coupling scheme, due to the hybridization with the p and d orbits (as shown in Sec. IV), i.e., the mixing of the different-parity single-particle states. The direct coupling interactions between the $p\frac{1}{2}$ and the $d\frac{5}{2}$ channels also give the important contribution to the hybridization, as discussed in Ref. [5] in detail. However, these interactions bring about much weaker

CRC effects than those between the $p\frac{1}{2}$ and $d\frac{3}{2}$ channels. *This is because the direct couplings between the single-particle orbits with the same spin direction are generally larger than those with the different spin directions*. The hybridization of the valence nucleon in the ^{12}C+^{13}C and ^{12}C+^{13}N systems is discussed in Sec. IV.

E. Dipole transitions due to the core-core Coulomb interaction

In the limit where we can ignore the ratio of the mass of the valence particle to the mass of the core nucleus, we can neglect the direct coupling interactions coming from the core-core interaction V_{CC}. Therefore, we have not taken into account these interactions in our OCRC analysis made so far [4,5,8,9]. However, if the *incident energy is lower than the Coulomb barrier*, there is a possibility that the Coulomb interaction between two core nuclei dominates the inelastic transitions, especially the dipole ($E1$) inelastic transition between the s and p orbit states *at distances outside the barrier*, where the effects of the nuclear interaction can be ignored.

We have performed the calculations of the excitation functions of the inelastic scattering cross sections going to the $s\frac{1}{2}$ channel with and without the core-core inelastic coupling interactions. The results are shown in Fig. 15 for the $^{12}\mathrm{C}+^{13}\mathrm{C}$ and $^{12}\mathrm{C}+^{13}\mathrm{N}$ systems. Even at energies below the Coulomb barrier (6 MeV) we do not observe clear difference between two curves even for the $^{12}\mathrm{C}+^{13}\mathrm{N}$ system, where the valence proton has a very long-tail wave function in the $s\frac{1}{2}$ state of $^{13}\mathrm{N}^*(\frac{1}{2}^+)$ as shown in Fig. 2. Namely, the core-core interaction does not cause appreciable effects on the excitation functions of the cross sections. One of the reasons is that the transition energy of the valence nucleon in $^{13}\mathrm{N}$ or $^{13}\mathrm{C}$ is somewhat large (2.36 MeV or 3.09 MeV) and hence there may be Q-value mismatch between the scattering waves before and after the transition.

In Fig. 16 we show the calculations for the $^{12}\mathrm{C}+^{13}\mathrm{N}$ system at $E_{\mathrm{c.m.}}=5.5$ MeV of partial cross sections of the inelastic scattering going to the $\frac{1}{2}^+$ channel with and without the core-core interaction, as functions of the total angular momentum J. We observe there also a small difference between the curves with and without the core-core interaction at around the grazing angular momentum. At higher angular momenta, however, we do not find the difference, even though the contribution of the Coulomb interaction to the scattering amplitudes seems to become important at larger distances.

In contrast to the results discussed above, important effects of the dipole ($E1$) transition due to the core-core Coulomb interaction have been reported for the scattering on $^{208}\mathrm{Pb}$ of the projectiles, $^{13}\mathrm{N}$ [10], $^{14}\mathrm{O}$ [10], $^{11}\mathrm{Be}$ [11,12], and $^{11}\mathrm{Li}$ [13,14]. In these cases the Coulomb interactions dominate completely over the nuclear interactions, and thus the Coulomb interactions induce strongly the dipole ($E1$) transitions in a wide range of the incident energy, as shown in their analyses. The core-core coupling interactions do not affect the other inelastic scatterings as well as the above $\frac{1}{2}^+$ inelastic scattering.

A note should be made on the present numerical calculations. Namely, in order to include the whole effects of the long-range Coulomb interaction in the calculations, we integrate the interactions until 250 fm of internuclear distance, although the results of the calculations show not so important contribution of higher partial waves as expected from this distance. As seen in Fig. 16, in fact, the $\sigma^{J\Pi}$ are negligibly small already at about $J=\frac{61}{2}$. However, if we cut the integral at a shorter distance (for example, $r=60$ fm), non-negligible fictitious contribution of the Coulomb interaction appears. This pretends that the convergence of the series of $\sigma^{J\Pi}$ ($J=\frac{1}{2},\frac{3}{2},\frac{5}{2},\ldots$) is very slow.

F. Fusion cross sections and the smearing effects of the valence nucleon on the molecular resonance phenomena observed in the $^{12}\mathrm{C}+^{12}\mathrm{C}$ system

In the calculation of the fusion cross sections (which are almost equal to the absorption cross sections at sub-barrier energies) shown in Fig. 17, we also observe such strong CRC effects as pointed out in Secs. III A–III D.

In order to see the reaction mechanism of the fusion, let us suppose the case where the extra neutron in the $^{12}\mathrm{C}+^{13}\mathrm{C}$ system does not make inelastic transitions and the
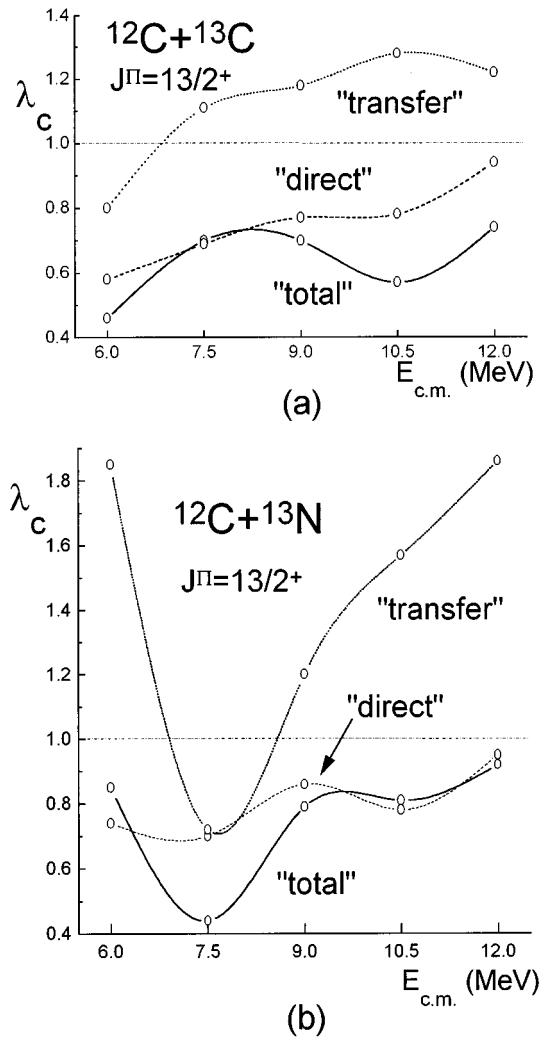

FIG. 13. As Fig. 12 for the four-channel OCRC calculations only with the transfer interactions (dotted curves), only with the direct coupling interactions (dashed curves), and with the full coupling interactions (transfer plus direct interactions) (solid curves) in the state of the total angular momentum $J^\Pi=\frac{13}{2}^+$. In the upper part of the figure the results for the $^{12}\mathrm{C}+^{13}\mathrm{C}$ system are shown and in the lower part those for the $^{12}\mathrm{C}+^{13}\mathrm{N}$ system.

elastic transfer of the neutron does not affect the absorption mechanism. Then, the fusion cross sections of such a $^{12}\mathrm{C}+^{13}\mathrm{C}$ system, i.e., those obtained by the one channel calculation for the $^{12}\mathrm{C}+^{13}\mathrm{C}$ system should almost agree with those of the $^{12}\mathrm{C}+^{12}\mathrm{C}$ system. This is observed in our calculation as shown in Fig. 17, where the one channel calculation of the fusion cross sections of the $^{12}\mathrm{C}+^{13}\mathrm{C}$ system are compared with those of the $^{12}\mathrm{C}+^{12}\mathrm{C}$ system [15]. It should be noticed that the cross sections observed in the $^{12}\mathrm{C}+^{12}\mathrm{C}$ system are reproduced by using the very weakly absorbing potential of the elastic channel of the $^{12}\mathrm{C}+^{13}\mathrm{C}$ system (see Table III).

It is well known that in the excitation function of the fusion cross sections of the $^{12}\mathrm{C}+^{12}\mathrm{C}$ system there are prominent structures [20,21]. These structures have been interpreted as due to the formation of the $^{12}\mathrm{C}+^{12}\mathrm{C}$ di-nuclear molecular resonance states [20,21,29,30], which are not included in the present analysis. Thus, we display the data only
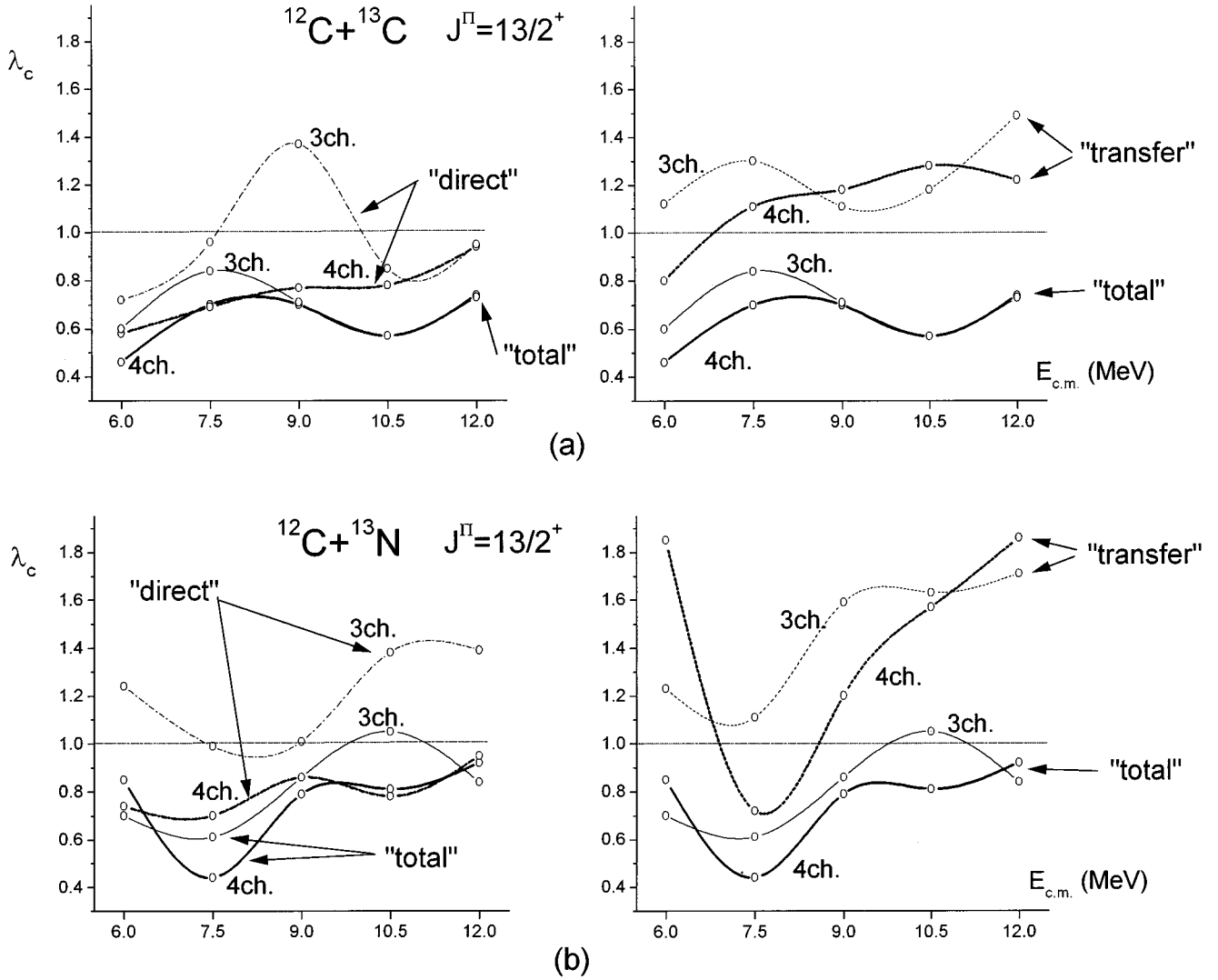
FIG. 14. As Fig. 12 for the comparison of the four-channel OCRC calculations (bold curves) with the three-channel calculations (slim curves). In the upper part of the figure the results for the ^{12}C+^{13}C system are shown and in the lower part those for the ^{12}C+^{13}N system. The dash-dotted curves display the calculations only with the direct interactions in the state of the total angular momentum $J^{\Pi}=\frac{13}{2}^{+}$ and the dotted curves only with the transfer interactions. The calculations with the full coupling interactions are shown by the solid curves.

at off-resonance energies in Fig. 17.

The OCRC fusion cross sections of the ^{12}C+^{13}C system are clearly enhanced as compared with the one-channel calculation especially at around $E_{c.m.}=5$ MeV, resulting in good agreement with the experimental data. Such enhancement of the sub-barrier fusion cross sections is caused by the strong couplings with the inelastic channels and by the absorption in these channels *where much stronger imaginary potentials than in the elastic channel exist as shown in Table III*.

In the ^{12}C+^{12}C system sharp and isolated resonances are observed, while in the ^{12}C+^{13}C system no such phenomena have been reported so far, although many experimental studies for this aim have been devoted [15,16,17,19]. Such sharp resonances have been explained by using the doorway state model [29,30] based on the ^{12}C+^{12}C inelastic channels, where very weakly absorbing potential between two ^{12}C nuclei are assumed, which is comparable with the imaginary part of the elastic-channel potential used in the ^{12}C+^{13}C OCRC calculation in this report.

Nevertheless, the lack of the resonances in the ^{12}C+^{13}C system can be explained by the above OCRC calculation, that is, the strong couplings to the inelastic channels introduce stronger absorption effects into the elastic channel of the ^{12}C+^{13}C system. Namely, the depth of the imaginary potential to be *effectively* used in the one-channel analyses for the ^{12}C+^{13}C and ^{12}C+^{13}N systems is considered to be so large as pointed out by Liénard *et al.* [$W(^{12}$C+^{13}N) $=3.0$ MeV and $W(^{12}$C+^{13}C)$=17.3$ MeV] [2]. Thus, the door-way-state molecular resonances (the total widths ≈ 100–200 keV) of the ^{12}C+^{12}C system which are strongly correlated to the elastic channel are smeared out almost completely by this absorption effect in the ^{12}C+^{13}C system (and also in the ^{12}C+^{13}N system).

IV. SUMMARY AND DISCUSSION WITH THE MOLECULAR-ORBITAL PICTURE OF THE VALENCE NUCLEON

We have made analysis for the elastic and inelastic scattering of the ^{12}C+^{13}N and ^{12}C+^{13}C systems with use of

the OCRC method, by taking into account of the core (^{12}C) exchange processes and by adopting the channels related to the valence nucleon states, $p\frac{1}{2}$, $s\frac{1}{2}$, $d\frac{5}{2}$, and $d\frac{3}{2}$ in the nuclei ^{13}N and ^{13}C. The parameters of the potential V_{CC} between two core nuclei are adjusted so as to reproduce the data of the angular distributions of the elastic and the inelastic scattering of the system ^{12}C$+^{13}$C at eight points of the energies from $E_{c.m.}=7.8$ to 12.72 MeV [9], and the fusion cross sections at energies below the Coulomb barrier [15].

The ^{12}C$+^{13}$N elastic scattering is analyzed by using the same optical potential V_{CC} as obtained in the analysis of the ^{12}C$+^{13}$C system. The result of the OCRC calculation reproduces the data of the elastic scattering measured at $E_{c.m.}=7.824$, 9.6, and 14.16 MeV nicely especially at forward angles, although the enhancement of the cross sections is not enough to trace the data at backward angles at higher energy.

We tested the calculation by adopting the potential V_{CC} for the ^{12}C$+^{13}$N system with the parameter of five times weaker depth of the imaginary potential, which has been introduced in the one-channel analysis by Liénard et al. [2]. However, this deteriorates clearly the result of the angular distributions at forward angles, indicating that the suggested weak-absorption potential is not likely in the present four-channel OCRC analysis.

Concerning the core-core potential V_{CC}, (i) the real parts used in the analysis depend on the parity of the total system, and (ii) the imaginary parts do on the channels of the elastic and inelastic scattering, that is, the depth of the imaginary part for the inelastic channels is much larger than that for the elastic channel. The above item (i) reflects the insufficient truncation of the space spanned by the channel wave functions probably.

On the other hand, the latter item (ii) may reflect the following two effects, i.e., (a) the emission and/or breakup processes of the valence nucleon and (b) the transitions to the channels not taken into account in this paper explicitly, which are followed by the fusion processes. The effect (a) possibly stems strongly from the inelastic channels where the valence nucleon is loosely bound and the wave functions extend far outside of the potential barrier. Thus, stronger absorption occurs in the inelastic channels than in the elastic channel. Such a kind of mechanism of the absorption in the excited channels has been also discussed recently by Hussein et al. [28] theoretically. The latter effects (b) may arise also strongly from the inelastic channels as compared with the effect of the transitions directly from the elastic channel to the channels mentioned above, i.e., the highly excited-state channels, because the inelastic channels are energetically closer to these excited-state channels. As these channels get to be closed at lower bombarding energies, the transitions in the peripheral region, i.e., the direct reactions from the inelastic channels to them may be suppressed at energies treated here. Thus, the colliding nuclei are trapped deeply within the potentials of the excited-state channels, and then fuse with each other into the compound nucleus emitting a proton, a neutron, and an alpha particle as shown in Fig. 1. This fusion mechanism may make a contribution also to the enhancement of the absorption in the inelastic channels. In the elastic channel, on the other hand, the existence of the weaker absorption potential is plausible from the view point that the ^{12}C$+^{12}$C system (core-core system of the ^{12}C
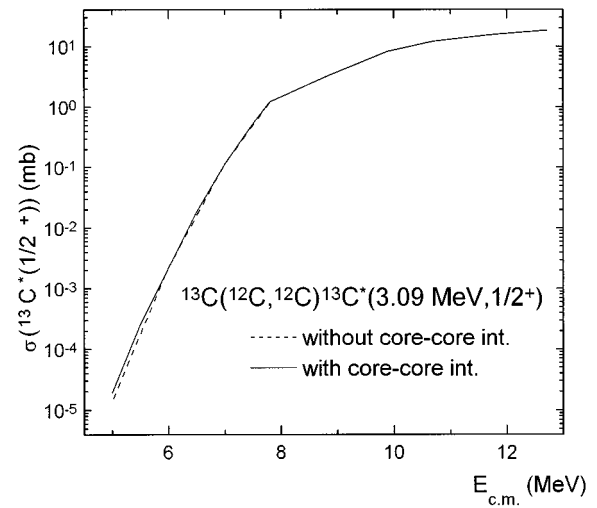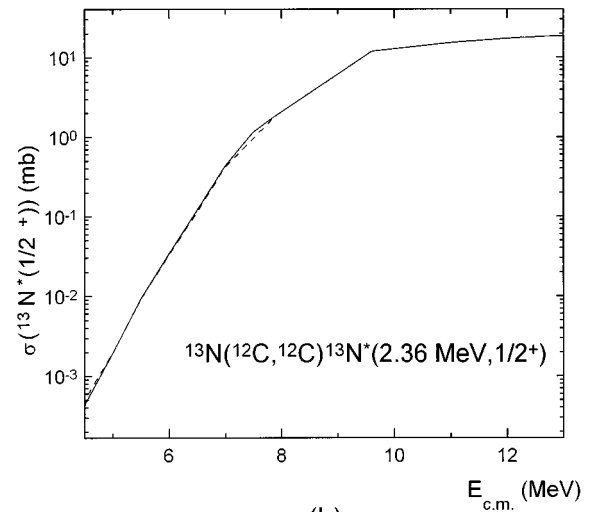
FIG. 15. Excitation functions for the integrated cross sections of the inelastic scattering ^{13}C(^{12}C, ^{12}C)^{13}C* (3.09 MeV, $\frac{1}{2}^{+}$) (upper part of the figure) and ^{13}N(^{12}C, ^{12}C)^{13}N* (2.36 MeV, $\frac{1}{2}^{+}$) (lower part of the figure). The solid and dashed curves show the OCRC calculations with and without the dipole ($E1$) coupling interactions due to the core-core interaction, respectively.

$+^{13}$C system) allows the molecular sharp resonances to exist with the large fractions of the decaying widths to the elastic channel [29,30].

We checked the effects of the dipole-transition interaction coming from the core-core potential V_{CC}. Our primary motivation is due to the very long tail of the wave function of the excited state ^{13}N*($\frac{1}{2}^{+}$, $2s\frac{1}{2}$), which may enhance the dipole ($E1$) transition induced by the core-core Coulomb interaction. However, the effects are so weak that no sizable change is seen in the calculations of the cross sections. This is in contrast to the strong dipole ($E1$) transitions observed in the heavy-ion scattering [10–14] on ^{208}Pb of ^{13}N, etc., at the incident energies of several tens MeV/u.

The CRC effects of the present four-channel OCRC calculations for the ^{12}C$+^{13}$N system as well as for the ^{12}C $+^{13}$C system were very strong, as has been already pointed out in the previous papers [4,5,8,9] with the three-channel
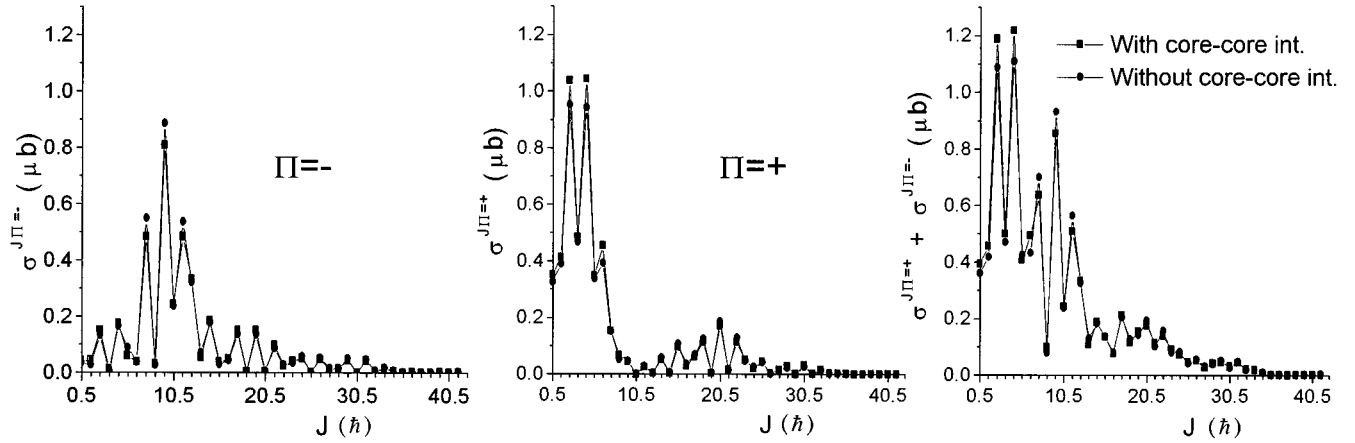
FIG. 16. Total angular momentum distributions of (a) the partial cross sections $\sigma^{J\Pi=-}$ (J: total angular momentum; Π: total parity), (b) $\sigma^{J\Pi=+}$, and (c) the sum of $\sigma^{J\Pi=-}$ and $\sigma^{J\Pi=+}$ at energy $E_{\text{c.m.}}=5.5$ MeV. The squares and the circles connected by the solid lines show the OCRC calculation with and without the dipole ($E1$) coupling interactions due to the core-core interactions, respectively.

($p\frac{1}{2}$, $s\frac{1}{2}$, and $d\frac{5}{2}$) OCRC analysis for the ^{12}C$+^{13}$C system. In the four-channel OCRC analysis, however, we had much stronger CRC effects due to the participation of the $d\frac{3}{2}$ channels into the CRC schemes. Namely the direct coupling interactions U_{ij} between the $d\frac{3}{2}$ and other channels, particularly between the $d\frac{3}{2}$ and $p\frac{1}{2}$ channels enhance the CRC effects of the system, as the result of stronger hybridization where the valence nucleon orbit is greatly distorted in the field of the approaching nucleus along the axis joining the two center of masses of two core nuclei.

The CRC effects for the ^{12}C$+^{13}$N and ^{12}C$+^{13}$C systems are compared with each other. Generally we observe stronger CRC effects in the latter than in the former. The molecular orbital picture can be employed to explain the above feature, if the CRC effects are determined *at each distance of the relative motion in an adiabatic approach*. Generally in the ^{12}C$+^{13}$N system the magnitudes of the coupling interactions between the $p\frac{1}{2}$ elastic and the $s\frac{1}{2}$, $d\frac{5}{2}$, or $d\frac{3}{2}$ inelastic channels at a fixed distance in the peripheral region are weaker than in the ^{12}C$+^{13}$C system. This is because the wave functions of the $s\frac{1}{2}$, $d\frac{5}{2}$, and $d\frac{3}{2}$ states of the valence nucleon in ^{13}N extend to larger distances than those in

^{13}C, as seen in Fig. 2. Thus, the mixing of the channel wave functions [see Eq. (15)] in the ^{12}C$+^{13}$N system, especially the *mixing of the different parity states causing the hybridization* is weaker than in the ^{12}C$+^{13}$C system.

The hybridization causes a specific configuration of the valence nucleon in the adiabatic ground states, i.e., the covalent molecular configuration where the density probability of the valence nucleon concentrates at the middle on the molecular axis of the systems, as seen in Fig. 18. As found from this figure, the concentration in the ^{12}C$+^{13}$C system is more pronounced than in the ^{12}C$+^{13}$N system, reflecting the result of stronger hybridization in the ^{12}C$+^{13}$C system.

The fusion cross sections of the CRC calculation of the ^{12}C$+^{13}$C system at energies below the Coulomb barrier are strongly enhanced as compared with those of the one-channel calculation. This is possibly explained by the following two reasons related to the covalent molecular-orbital formation of the valence neutron. (i) One of them is that the barrier height of the adiabatic potential $\mathscr{V}_{p=1}(r)$ corresponding to the energetically lowest (covalent molecule) state is lowered as compared to the diagonal potential $U_{11}(r)$ of the incident channel in the original OCRC basis. This is shown
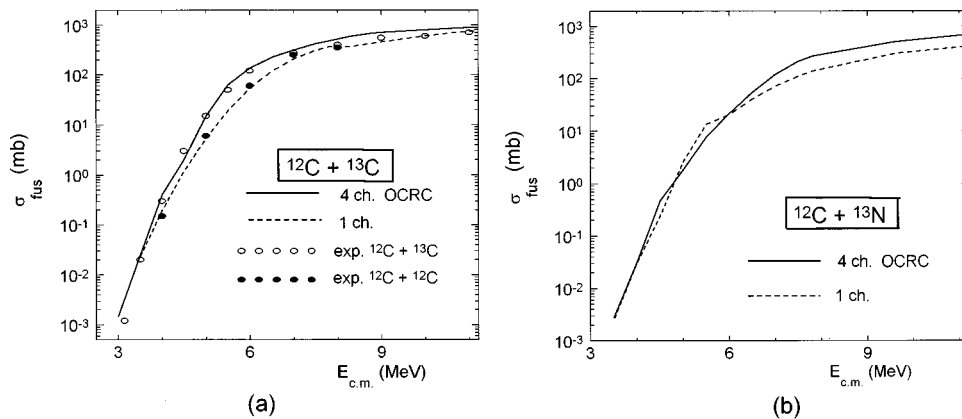

FIG. 17. (a) Absorption cross sections of the ^{12}C$+^{13}$C and ^{12}C$+^{12}$C systems (left part of the figure), and (b) those of the ^{12}C$+^{13}$N system (right part of the figure). The solid curves show the four-channel OCRC calculations and the dashed curves the one-channel calculations. The open circles in the left figure show the experimental data of the fusion cross sections for the ^{12}C$+^{13}$C system, and the closed circles the data for the ^{12}C$+^{12}$C system which are picked up from Ref. [15] at off-resonance energies for the quasimolecular states.
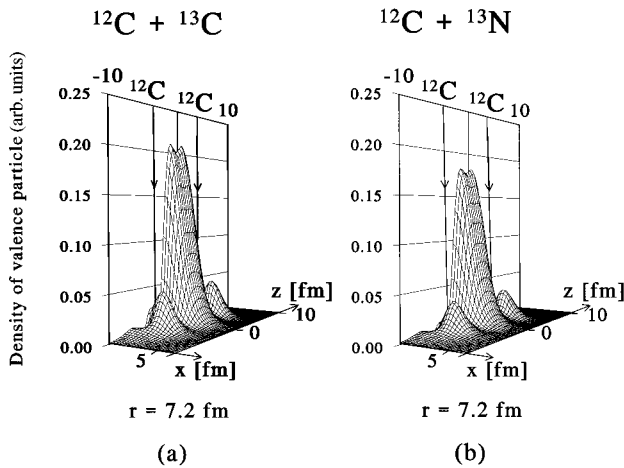
FIG. 18. Density distributions of the valence particles in the ground RMO (rotating molecular orbital: see the text) states at the internuclear distance $r = 7.8$ fm (a) in the $^{12}C + ^{13}C$ system and (b) in the $^{12}C + ^{13}N$ system. The positions of the core nuclei for the respective systems are marked by arrows.
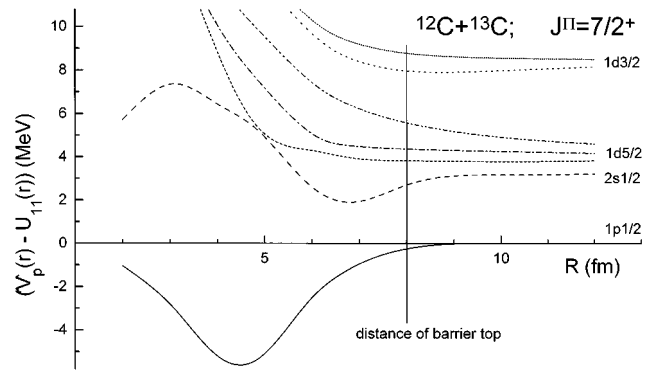

FIG. 19. Adiabatic potential diagram for the $^{12}C + ^{13}C$ system. The respective curves show the quantities $\mathcal{V}_p(r) - U_{11}(r)$, where $\mathcal{V}_p(r)$ is the adiabatic potential of the RMO state "p" defined by Eq. (16) in the text and $U_{11}(r)$ the channel-diagonal interaction in the original OCRC basis functions. It is found that the adiabatic potential of the ground RMO state is much lower than the $U_{11}(r)$ in the interaction region.

in Fig. 19, where the potentials $[\mathcal{V}_p(r) - U_{11}(r); \; p = 1,\ldots,n]$ are shown as a function of the radial distance r. The difference $[\mathcal{V}_{p=1}(r) - U_{11}(r)]$ is about -0.5 MeV at the distance $r \approx 8.0$ fm where the potential has the barrier top. This decrease causes the enhancement of the fusion cross sections observed in the OCRC calculation. (ii) The other reason is that the depth $\mathcal{W}_{p=1}(r)$ of the imaginary potential for the adiabatic state of the covalent molecular configuration ($p=1$) is deeper than the depth of the imaginary potential $W_{i=1}(r)$ of the incident channel ($i=1$) of the original OCRC basis, because of the following relation:

$$\mathcal{W}_{p=1}(r) = \sum_{i=1}^{n} W_i(r) A_{ip=1}^2(r) < W_{i=1}(r);$$

$$\text{if } W_j(r) < W_1(r) \quad \text{for } j \geq 2,$$

where $A_{ip=1}(r)$ are the transformation coefficients for the adiabatic state $p=1$ defined by Eqs. (15) and (16). We have employed stronger depth of the $W_j(r)$ ($j \geq 2$) for the inelastic channels than that for the elastic channel, as listed in Table III. Therefore, the depth of the imaginary potential $\mathcal{W}_{p=1}(r)$ for the adiabatic state $p=1$ is much deeper than that of the $W_{i=1}(r)$ for incident channel of the original OCRC bases. This also causes the enhancement of the fusion cross sections.

In the $^{12}C + ^{13}N$ system, on the other hand, such enhancement has been not clearly observed at energies below the Coulomb barrier. This is probably because the CRC effects of this system is weaker than that of the $^{12}C + ^{13}C$ system, as discussed in Sec. III C.

We have also pointed out that the absorption mechanism in the $^{12}C + ^{13}C$ system is related to the molecular resonance phenomena observed in the $^{12}C + ^{12}C$ system where a weak absorption potential exists. In the $^{12}C + ^{13}C$ system, however, the couplings to the inelastic channels make the absorption stronger. Thus, the sharp resonances of the $^{12}C + ^{12}C$ system are smeared out completely in the $^{12}C + ^{13}C$ system due to this CRC mechanism.

Finally we again emphasize that our OCRC model explains, using the charge symmetric reaction mechanism with the strong CRC effects, the experimental data for the elastic scattering of ^{13}N on ^{12}C measured by Liénard et al. [2] as well as those for the elastic and inelastic scattering of ^{13}C on ^{12}C measured by Voit et al. [9]. In our calculation such a big loss of the charge symmetry as pointed out by Liénard et al. [2] has not been found. The loss may come from insufficient space truncation with respect to two-fragment direct-reaction channels which are explicitly treated in this paper. It is not important to pay special attention to the difference of the decay schemes of the compound nuclei corresponding to the respective scattering systems in order to explain the charge asymmetry between the $^{12}C + ^{13}N$ and $^{12}C + ^{13}C$ systems.

ACKNOWLEDGMENTS

[1] *Proceedings of the Third International Conference on Radioactive Nuclear Beams*, East Lansing, Michigan, 1993, edited by D. J. Morrissey (Frontières, Gir-sur-Yvette, 1993); Proceedings of the Fourth International Conference on Radioactive Nuclear Beams, Omiya, Japan, 1996, edited by S. Ku-

bono, T. Kobayashi, and I. Tanihata (unpublished).
[2] E. Liénard, D. Baye, Th. Delbar Descouvemont, P. Duhamel, W. Galster, M. Kurokawa, P. Leleux, I. Licot, P. Lipnik, C. Michotte, T. Motobayashi, A. Ninane, J. Vanhorenbeeck, and J. Vervier, Phys. Rev. C **52**, 775 (1995).

[3] W. von Oertzen and H. G. Bohlen, Phys. Rep., Phys. Lett. **19C**, 1 (1975).

[4] W. von Oertzen and B. Imanishi, Nucl. Phys. **A424**, 262 (1984).

[5] B. Imanishi and W. von Oertzen, Phys. Rep. **155**, 29 (1987).

[6] J. Y. Park, W. Scheid, and W. Greiner, Phys. Rev. C **6**, 1565 (1972); Phys. Rev. C **20**, 188 (1979).

[7] W. Greiner, J. Y. Park, and W. Scheid, *Nuclear Molecules* (World Scientific, Singapore, 1995) p. 249; see also references to prior work therein.

[8] B. Imanishi and W. von Oertzen, Phys. Lett. **87B**, 188 (1979); W. von Oertzen, B. Imanishi, H. G. Bohlen, T. Treu, and H. Voit, Phys. Lett. **93B**, 21 (1980).

[9] H. Voit, N. Bischof, W. Tiereth, I. Weitzenfelder, W von Oertzen, and B. Imanishi, Nucl. Phys. **A476**, 491 (1988).

[10] T. Motobayashi, T. Takei, S. Kox, C. Perrin, F. Merchez, D. Rebreyend, K. Ikei, H. Murakami, Y. Ando, N. Iwasa, M. Kurokawa, S. Shirato, J. Ruen, T. Ichihara, T. Kubo, N. Inabe, A. Goto, S. Kubono, S. Shimoura, and M. Ishihara, Phys. Lett. B **264**, 259 (1991).

[11] R. Anne, D. Bazin, R. Bimbot, M. J. G. Borge, J. M. Corre, S. Dogny, H. Emling, D. Guillemaud-Mueller, P. G. Hansen, P. Hornshj, P. Jensen, B. Jonson, M. Lewitowicz, A. C. Mueller, R. Neugart, T. Nilsson, G. Nyman, F. Pougheon, M. G. Saint-Laurent, G. Schrieder, O. Sorlin, and K. Wilhelmsen-Rolander, Z. Phys. A **352**, 397 (1995).

[12] T. Nakamura, T. Motobayashi, Y. Ando, A. Mengoni, T. Nishio, H. Sakurai, S. Shimoura, T. Teranishi, Y. Yanagisawa, and M. Ishihara, *Abstract Book of the Forth International Conference on Radioactive Nuclear Beams*, Omiya, Japan, 1996, edited by RNB4 Organizing Committee, Phys. Lett. B **394**, 11 (1997).

[13] S. Shimoura, T. Nakamura, M. Ishihara, N. Inabe, T. Kobayashi, T. Kubo, R. H. Siemssen, I. Tanihata, and Y. Watanabe, Phys. Lett. B **348**, 29 (1995); S. Typel and G. Baur, Nucl. Phys. **A573**, 486 (1994).

[14] C. A. Bertulani, L. F. Canto, and M. S. Hussein, Phys. Rep. **226**, 28 (1993).

[15] B. Dasmahapatra, B. Cujec, and F. Lahlou, Nucl. Phys. **A384**, 257 (1982).

[16] R. A. Dayras, R. G. Stokstad, Z. E. Switkowski, and R. M. Wieland, Nucl. Phys. **A265**, 153 (1976).

[17] M. L. Chaterjee, L. Potvin, and B. Cujec, Nucl. Phys. **A333**, 273 (1980).

[18] L. Corradi, in Proceedings of International Workshops on Heavy-Ion Fusion Exploring the Variety of Nuclear Properties, Padua, Italy, 1994, edited by A. M. Stefanini *et al.* (unpublished), p. 34, see references to prior work therein.

[19] L. T. Chua, A. Gobbi, M. W. Sachs, D. Shapira, R. Wieland, and D. A. Bromley, Nuovo Cimento A **47**, 430 (1978); L. T. Chua and D. A. Bromley, Nuovo Cimento A **47**, 443 (1978).

[20] D. A. Bromley, J. A. Kuehner, and E. Almqvist, Phys. Rev. Lett. **4**, 365 (1960); Phys. Rev. **123**, 878 (1961); E. Almqvist, D. A. Bromley, and J. A. Kuehner, Phys. Rev. Lett. **4**, 515 (1960); E. Almqvist, D. A. Bromley, J. A. Luehner, and D. Whalen, Phys. Rev. **130**, 1140 (1962).

[21] K. A. Erb, and D. A. Bromley, in *Treatise on Heavy-Ion Science*, edited by D.A. Bromley (Plenum, New York, 1984), Vol. 3, p. 201; see also references to prior work therein.

[22] N. Austern, Y. Iseri, M. Kamimura, M. Kawai, G. Rawitcher, and Y. Yahiro, Phys. Rep. **154**, 125 (1987), see also references to prior work therein.

[23] Y. Sakuragi, M. Yahiro, and M. Kawai, Prog. Theor. Phys. Suppl. **89**, 136 (1986).

[24] W. von Oertzen, Th. Wilpert, B. Bilwes, L. Stuttge, J. L. Ferrero, J. A. Luiz, I. J. Thompson, and B. Imanishi, Z. Phys. A **353**, 373 (1996).

[25] The accuracy of the OCRC formalism with this approximation was checked by making the comparison between the calculation with this method and the full finite-range DWBA calculation for the transfer reaction ^{13}C[^{12}C, ^{13}C*(3.08 MeV, $\frac{1}{2}^{+}$)] ^{12}C at energies near the Coulomb barrier. The errors were within 10 percent (unpublished): This approximation and the recoil effects themselves are discussed in detail in an article on the treatment for the recoil effects with the orthogonalized coupled-reaction-channel theory; it will be published somewhere.

[26] I. J. Thompson, Comput. Phys. Rep. **7**, 169 (1988), see also references to prior work therein.

[27] S. Cohen and D. Kurath, Nucl. Phys. **A101**, 1 (1967).

[28] M. S. Hussein, M. P. Pato, and A. F. R. de Toledo Piza, Phys. Rev. C **51**, 846 (1995).

[29] B. Imanishi, Nucl. Phys. **A125**, 33 (1969).

[30] Y. Abe, Y. Kondo, and T. Matsuse, Prog. Theor. Phys. Suppl. **68**, 303 (1980).